ISSN 0016-7029, Geochemistry International, 2024, Vol. 62, No. 5, pp. 466–492. © Pleiades Publishing, Ltd., 2024.

Sources and Formation Parameters of the Melts of Granitoids of the Khokhol–Repyevka Batholith in the Volga–Don Orogen, East European Craton

M. E. Petrakova[a, *], A. B. Kuznetsov[a, b], Sh. K. Baltybaev[a, b], V. M. Savatenkov[a, b], R. A. Terentiev[c], and K. A. Savko[c]

[a] *Institute of Precambrian Geology and Geochronology, Russian Academy of Sciences, St. Petersburg, 199034 Russia*

[b] *St. Petersburg State University, St. Petersburg, 199034 Russia*

[c] *Research Institute of Geology, Voronezh State University, Voronezh, 394006 Russia*

**e-mail: maribya@mail.ru*

Received November 7, 2023; revised January 23, 2024; accepted January 24, 2024

Abstract—The paper discusses the sources of melts and their formation parameters for granitoids of the Khokhol–Repyevka batholith that compose the Don terrane of the Volga–Don orogen in the East European craton. The batholith is made up of granitoids of three types: Pavlovsk granitoids (quartz monzonites–granites, mostly without pyroxenes), Potudan granitoids (quartz monzogabbro–granodiorites containing pyroxene), and hybrid ones (quartz monzodiorites, monzonites, and quartz monzonites). These three types of rocks occur together and have a similar age of 2050–2080 Ma, similar geochemical characteristics (high contents of Ba, Sr, and highly fractionated REE patterns with $Gd_N/Yb_N = 2–11$), but differ in petrographic and isotopic geochemical parameters. The initial isotope characteristics of the sources of the Pavlovsk-type rocks are $\varepsilon_{Nd}(t) = +0.2$ to -3.7 and $Sr_i = 0.70335$, those of the Potudan type are $\varepsilon_{Nd}(t) = -1.7$ to -3.8, $Sr_i = 0.70381–0.70910$, and the hybrid rocks have $\varepsilon_{Nd}(t) = -8.8$, $Sr_i = 0.70596$. In addition to granitoids, the batholith was found out to host two types of leucogranite dikes. One of them is characterized by $\varepsilon_{Nd}(t) = -3.8$ and fractionated HREE patterns ($Gd_N/Yb_N = 2.1–3.8$) and could be formed as a result of the deep differentiation of Pavlovsk-type magma. The other type has $\varepsilon_{Nd}(t) = -7.8$ and less fractionated HREE patterns ($Gd_N/Yb_N = 1.1–1.6$), which likely resulted from the melting of a crustal source at shallow depths. The Rb–Sr isotope-geochemical characteristics of rocks of the Pavlovsk and Potudan types indicate that their melts were derived from different sources. The melts of the Khokhol–Repyevka batholith were thus derived from at least three sources: (1) lower (or buried oceanic) crust of predominantly mafic composition and/or enriched mantle, which was metasomatized in the Proterozoic, whose involvement is reflected in the composition of the Pavlovsk granitoids; (2) an enriched mantle source, which was likely subcontinental lithospheric mantle (SCLM) that had been metasomatized during an earlier stage of the geological development of the region, specific of the Potudan-type monzonitoids; and (3) Archean crust consisting mostly of TTG gneisses and metasediments, which underwent melting and participated in the formation of some of the leucogranite dikes and hybrid rocks. The results of thermodynamic modeling indicate that the mixing of two melts contrasting in composition (Potudan-type mafic and Pavlovsk-type intermediate–felsic) could form only some of the hybrid rocks. The others could be formed by mafic melt contaminated with anatectic melts derived from the Archean crust of the Kursk block.

Keywords: granitoids, gabbroids, magma hybridization, SCLM, thermodynamic modeling, Don terrane, Paleoproterozoic

DOI: 10.1134/S001670292470023X

INTRODUCTION

Geodynamic processes during the accretion of cratons thickened the crust as a result of continental collision, produced juvenile crust by means of newly coming portions of mantle magmas, thinned the lithosphere, and brought about asthenospheric upwelling (Sylvester, 1989; Black and Liegéois, 1993; Bonin et al., 1998; Zhao et al., 2002; Condie, 2013). The transition from the compressional (syn- to postcollisional) to extensional (postcollisional) regimes was associated with the mixing of melts coming from several magma sources and the contamination of these melts via melting ancient metamorphic and sediment rocks. Subduction and collision at cratonic peripheries formed orogenic belts that hosted granitoids of different mineralogical and geochemical composition depending on the proportions of melted material from different sources (Brown et al., 1984; Sylvester, 1989; Frost et al., 2001).

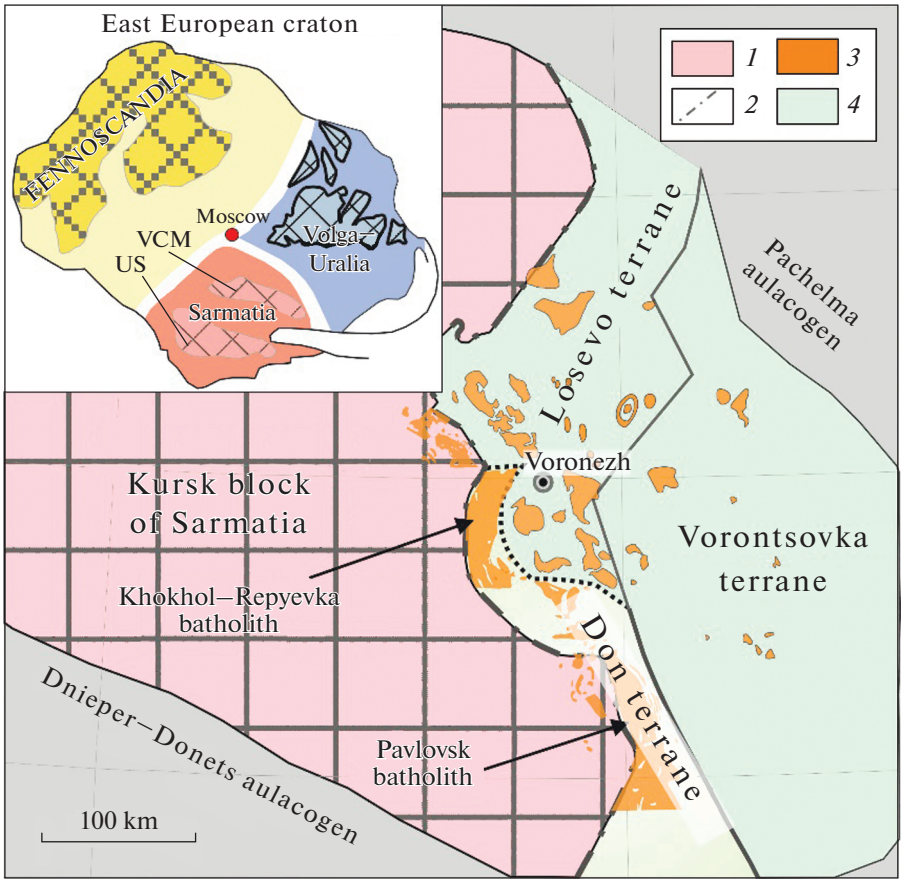

Fig. 1. Schematic geological map of the Precambrian basement of the Kursk block of Sarmatia and the Volga–Don orogen: (*1*) Archean basement; (*2*) boundary between the Proterozoic Volga–Don orogen; (*3*) granite complexes; (*4*) metamorphic rocks (modified after Terentiev, 2014; Savko et al., 2017; Terentiev et al., 2020). The inset shows the East European craton with its basement inliers in the Archean Sarmatia block: *VCM* is the Voronezh crystalline massifs, and *US* is the Ukrainian shield (Gorbatschev and Bogdanova, 1993, Bibikova et al., 2015; Fedotova et al., 2019).

The Volga–Don orogen (VDO) was formed by the accretion of Paleoproterozoic ensimatic and sialic arcs (Vorontsovka, Losevo, and Don terranes) to the Kursk continental block of Sarmatia during the accretion of the Volga–Ural protocontinent at 2.1–2.07 Ga (Shchipansky et al., 2007; Bibikova et al., 2009; Terentiev, 2014; Shchipansky and Kheraskova, 2023) (Fig. 1). The collision of Sarmatia and Volga–Uralia was, in turn, a link in the chain of a global Paleoproterozoic event: the most ancient Archean crustal blocks were combined into the Nuna–Columbia supercontinent (Meert, 2012; Chaves, 2021).

The Khokhol–Repyevka batholith is one of the largest batholiths in the western part of VDO. This batholith is dominated by granitoids of the Pavlovsk complex. Recently obtained petrographic–mineralogical and geochemical data on the rocks and the U–Pb (SIMS) zircon dates of the rocks (Petrakova and Terentiev, 2018; Terentiev et al., 2020; Petrakova et al., 2022a) indicate that the batholith is made up of rocks of three groups, which are similar in age but different in petrochemistry.

(1) The granitoids of the Pavlovsk type (2076 ± 10 Ma) broadly vary in composition (from quartz monzodiorite and granodiorite to quartz monzonite and granite). Zircon in these rocks shows thin oscillatory zoning and occasionally contains inherited cores (Terentiev et al., 2020). The rocks are mostly magnesian, belong to the normal-alkalinity to mildly alkaline series, are rich in LILE (first of all, Ba and Sr), and have strongly fractionated HREE patterns and broadly varying $\varepsilon_{Nd}(t) = +0.2$ to -4.2. These rocks are thought to have been formed via the melting of an enriched mafic garnet-bearing source contaminated with the material of the Paleoproterozoic and ancient Archean crust, as follows from the inherited zircon cores (Terentiev et al., 2020).

(2) Quartz monzogabbro–granodiorites of the Potudan type (2056 ± 7 Ma), which are rich in iron and alkalis (first of all, potassium in mafic types) and belong to the mildly alkaline series, and this makes these rocks different from the Pavlovsk-type granitoids. The rocks have strongly fractionated HREE patterns, are rich in LILE, and are strongly enriched in Ba and Sr. Their zircon shows coarse zoning or banding (Petrakova et al., 2022a), as is typical of zircon crystallizing from magmatic gabbroid melts (Corfu et al., 2003).

(3) Hybrid rocks (2068 ± 6 Ma), which are found only sporadically, significantly vary in composition from monzodiorite to monzogranite and granite, are sometimes ferroan and sometimes magnesian, and have trace-element compositions intermediate between those in the rocks of the former two groups. Zircon in the rocks hosts coarsely zoned cores overgrown with thinly zoned rims (Terentiev et al., 2020; Petrakova et al., 2022a). The rocks show evidence of mixing of mafic and felsic magmas: the normal and inverse zoning of their plagioclase, oikocrysts of quartz and/or potassic feldspar, and schlieren of mafic minerals (Petrakova and Terentiev, 2018). One sample of the quartz monzonite was found out to have a low $\varepsilon_{Nd}(t) = -8.7$ (Terentiev et al., 2020).

The rocks of the three group occur near one another, are similar in age, and crystallized under similar parameters: pressures of 2.7–3.2 kbar, liquidus temperatures of 1100–980°C, and subliquidus temperatures of 800–700°C (Petrakova and Terentiev, 2018). The melts are thought to have been derived from an enriched heterogeneous source with high concentrations of alkalis, LILE, and LREE. A contribution of a mantle component follows from that some of the rocks are poor in SiO_2, contain elevated concentrations of MgO, Cr, Ni, and Ti, and have high Sr/Y, $(La/Yb)_N$, and $(Dy/Yb)_N$ ratios, which suggest that the magmas were derived at significant depths and crystallized at high temperatures (Petrakova et al., 2022a).

The Khokhol–Repyevka batholith also hosts gray and pinkish gray aplitic leucogranite dikes. Their genesis and relations to other rocks of the batholith are uncertain.

Available geochemical and Sm–Nd isotope data are still insufficient to unambiguously interpret the sources of the granitoids of the Khokhol–Repyevka batholith. To clarify these issues, we have studied the Rb–Sr isotope systematics and applied techniques of thermodynamic modeling of magmatic mineral-forming processes with a control of isotope ratios in the magma (a) at the crystallization of minerals in models for mixing different melts and (b) at the contamination with/assimilation of the host rocks. Our principal aim is to test the validity of mixing and hybridism models with reference to the origin of the Khokhol–Repyevka batholith and to identify the probable melt sources. Another aim of our study was to understand the nature of the leucogranite dike suite. Detailed data obtained by studying the granitoids and leucogranites should hopefully deepen our understanding of Paleoproterozoic crust-building processes and the role of mantle processes in the origin of the regional geological complexes.

GEOLOGICAL STRUCTURE OF THE VOLGA–DON OROGEN

The Volga–Don orogen (VDO) was produced in relation to subduction–collision processes at 2.2–2.1 Ga. It is thought that the hypothetical Paleoproterozoic ocean included ensimatic and ensialic arcs, and their mutual collision and accretion when the ocean closed produced the Volga–Don orogen (Shchipansky et al., 2007; Bibikova et al., 2009; Bogdanova et al., 2005; Samsonov et al., 2016; Terentiev and Santosh, 2020). The mergence of the Archean Sarmatia and Volga–Uralia blocks that resulted from the closure of the ocean induced folding and metamorphism of the Paleoproterozoic rocks of the Kursk block and the Losevo and Vorontsovka terranes.

The Don, Losevo, and Voronstovka terranes, which are separated by large regional faults from one another, were distinguished in VDO based on drilling materials and geophysical data (Mints et al., 2017). The Volga–Don orogen was traced for 700 km from Ryazan to Volgograd. All VDO structures are unconformably overlain by a cover of Phanerozoic sedimentary rocks 0.5 to 500 m thick. VDO is bounded by the Archean Kursk block in the west and by the buried structures of the Archean Azov block in the south. In the east, VDO is bounded by the Paleoproterozoic Tersinskii belt of metamorphosed volcanic rocks and the Southern Volga supracrustal complex of Volga–Uralia (Bibikova et al., 2009; Bogdanova et al., 2005). The northern limitation of VDO is uncertain, and VDO may be truncated there by Mesoproterozoic structures of the Central Russia belt. VDO structures are overlain by Meso- to Neoproterozoic rocks of the Pachelma aulacogen in the north and by rocks of the Dnieper–Donets aulacogen and Caspian depression in the south (Fig. 1).

The Don terrane was distinguished relatively recently (Savko et al., 2014; Terentiev, 2018; Terentiev et al., 2020). The volcanic–sedimentary rocks of the Don Group are fine-grained biotite gneisses, amphibolites, marbles, and calciphyres. The metavolcanic rocks (basalts and andesites) belong to the calc-alkaline high-K series and are classified into high-Fe and high-Mg types. The volcanic rocks of the Don Group are similar to the calc-alkaline rocks of the Losevo Group but differ from them in containing higher K and Th concentrations (Terentiev, 2018). The sedimentary material of the Don Group was accumulated in a marine basin, as also follows from that beds of marbles and calc-silicate rocks (whose protoliths were limestone and marl) occur among these rocks. The rocks of the Don Group are ubiquitously cut by the largest batholiths of Paleoproterozoic (2076–2056 Ma) granitoids (Savko et al., 2014; Terentiev, 2016; Terentiev et al., 2020; Petrakova et al., 2022a). Although no data on the age of the sedimentary rocks of the Don Group are available so far, similarities between them and the metamorphosed calc–silicate rocks of the Paleoproterozoic Central Azov Group in the Azov block, as well as the fact that the former group is cut by granitoids dated at 2052 ± 5 Ma (Kuznetsov et al., 2019), suggest that the rocks can be provisionally correlated. If so, the Paleoproterozoic Sr chemostratigraphic age of the

metacarbonate rocks (older than 2230 Ma) and the Nd model age (2310–2340 Ma) of the Temryuk Formation can be used as a provisional date for the accumulation of the sedimentary material of the Don Group.

The Losevo terrane is made up of a bimodal metavolcanic rock series with tholeiites comagmatic with the gabbroids of the Rozhdestvenskii complex and the basalt–andesite–dacite series with variable proportions of sedimentary and volcanic–sedimentary rocks (~2.14 Ga; Terentiev et al., 2014, 2017). The metamorphic rocks of the Losevo Group are cut across by intrusions of tonalite–trondhjemite–granodiorite and trondhjemite–granodiorite–granite composition.

The Vorontsovka terrane consists of turbidite-type sediments, which compose flyschoid sandy–shale sedimentary sequences (Savko et al., 2011; Terentiev and Santosh, 2016) that are, in turn, cut by numerous bodies of ultramafic–mafic rocks and small S- and A-type granite intrusions (Savko et al., 2014). All intrusive rocks of the Vorontsovka and Losevo terranes have positive $\varepsilon_{Nd}(t)$ values.

The TIMS monazite age of the high-temperature low-pressure (HT/LP) metamorphic processes in the Kursk block and Vorontsovka terrane is 2067 ± 9 Ma (Savko et al., 2018), which corresponds to the most probable emplacement age (2050–2080 Ma) of a large volume of the mafic and granite intrusions. The metamorphic temperatures and pressures were evaluated at 430–750°C and 3–5 kbar, respectively (Savko et al., 2015). No reliable and unambiguous estimates of the *P–T* metamorphic parameters are still known for the Don and Losevo terranes because their rocks contain no mineral assemblages suitable for reasonably accurate evaluations. As of now, it can only be declared that the gneisses and amphibolites of the Don terrane are metamorphosed to the amphibolite facies, whereas the metamorphic grade of such rocks in the Losevo terrane corresponds to the epidote-amphibolite facies (Savko et al., 2015; Terentiev, 2018).

The Khokhol–Repyevka and Pavlovsk batholiths together occupy an area of approximately 4000 km^2 (Fig. 1). The Pavlovsk complex additionally includes a group of spatially separated massifs in the central part of the Don terrane and in the Kursk block (Fig. 1). The rocks of this complex range from quartz monzodiorite to leucogranite.

The following three types of granitoids are distinguished in the Khokhol–Repyevka batholith according to the structural setting and composition of these rocks: (1) granitoids of the Potudan type, which are mostly quartz monzogabbro–monzodiorite and granodiorite containing clinopyroxene; (2) granitoids of the Pavlovsk type, which are porphyritic quartz (monzogabbro)–monzodiorite, quartz monzonite, granodiorite, and granite that commonly contain no pyroxenes; and (3) granitoids of a hybrid type, which are rocks with discernible evidence of magma mixing and that show lineation or foliation.

The central part of the Don terrane hosts the Liski complex of A-type granites, which was produced during a later pulse of magmatic activity in the Paleoproterozoic (2064 ± 14 Ma) (Terentiev, 2016). The massive granites of the Liski pluton crosscut the Pavlovsk-type granites and show cutting relations with them.

The final pulse of magmatic activity of the Khokhol–Repyevka batholith produced pink fine-grained leucogranite dikes ranging from a few centimeters to a few meters in thickness. These dikes cut across all other geological bodies.

MINERALOGY AND PETROGRAPHY OF ROCKS OF THE KHOKHOL–REPYEVKA BATHOLITH

The Potudan type of rocks is represented by samples from drillhole core material from the Potudan massif (core material recovered by Drillholes 8003 and 6418) (Figs. 2, 3a) and some massifs north of this pluton (Drillholes 7577, 7578, 7569, 7580, 7583, and 7586). As seen by the naked eye, the rocks are dark gray to gray and pinkish gray massive fine- to medium-grained. They typically contain well preserved clinopyroxene or its relics, which are replaced by amphibole and/or biotite (most commonly aggregates of amphibole and biotite). The modal composition of these rocks and the average anorthite concentrations in the plagioclase of these rocks classify them as quartz monzogabbro, quartz monzogabbro-diorite, monzodiorite, and granodiorite. The major rock-forming minerals are plagioclase (An_{50} to An_{30}, 32–54%; here and below, the contents are given in vol %), potassic feldspar (mostly microcline, 6–22%), biotite (9–22%), magnesian hornblende (0.5–12%), quartz (5–12%), and clinopyroxene (diopside, 5–10%). The accessory minerals are magnetite (up to 6%), ilmenite, apatite, titanite, titanomagnetite, zircon and occasionally found pyrrhotite, pyrite, and chalcopyrite.

The Pavlovsk-type granitoids are classified make up two phases (Egipko, 1971; Terentiev and Savko, 2017). The Pavlovsk-type rocks of phase 1 were found in large heterogeneous massifs and make up the bulk of the batholiths. These are pink to gray fine- to medium-grained and pink to red porphyritic, often coarse-grained granitoids. The phase-2 granitoids cut the phase-1 and supracrustal rocks and occur as small bodies and veins of leucogranites, aplites, and pegmatites. According to their modal composition, the Pavlovsk-type rocks are classified with quartz monzodiorite, quartz monzonite, monzogranite, granodiorite, and more rarely, monzodiorite, monzonite, quartz syenite, and syenogranite. The major rock-forming minerals of these rocks are plagioclase (An_{35} to An_{25}, 41–50%), potassic feldspar (22–35%), amphibole (magnesian hornblende and edenite; 3–10%), quartz (18–26%), and biotite (3–10%). The accessory minerals (3–5%)

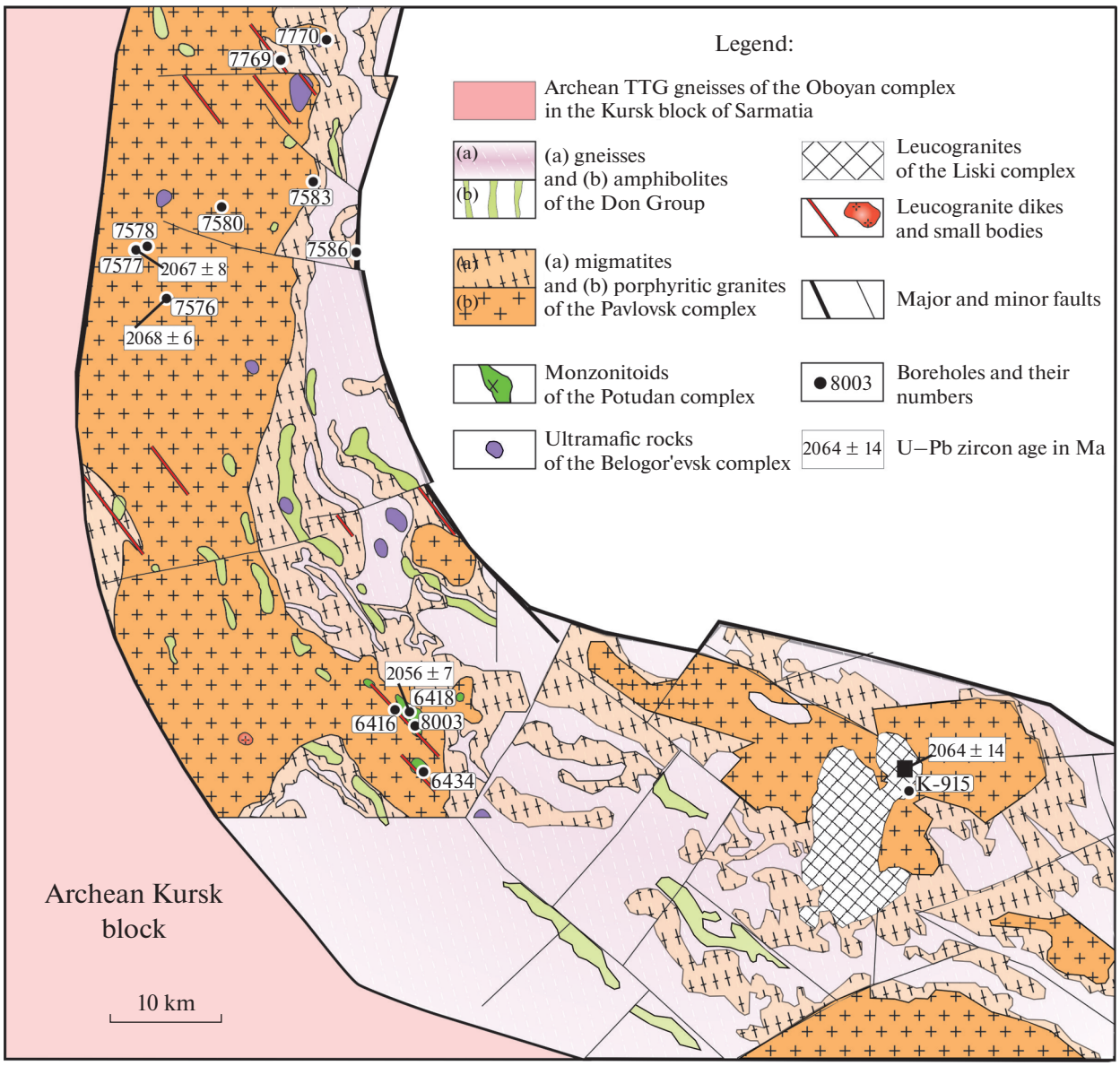

Fig. 2. Schematic geological map of the Khokhol–Repyevka batholith and the central part of the Don terrane.

are magnetite, titanite, apatite, zircon, ilmenite, and epidote (Fig. 3b).

The rocks of the hybrid type consist of the same rock-forming minerals as the granites of the former two types and combine features of both the Potudan type gabbro-diorites and the Pavlovsk-type granitoids (Figs. 3c, 3d). The mineralogical and petrographic indications of their hybrid nature involve oriented grains of mafic minerals and phenocrysts set in a fine-grained or often inequigranular groundmass.

The dikes are mostly made up of fine- to medium-grained massive leucogranite, which is sometimes aplitic. These rocks are dominated by quartz (25–45%), plagioclase (30–40%), potassic feldspar (32–52%), biotite (2–5%), and muscovite (+ chlorite) (0.2–1.3%) and often contain myrmekites (Figs. 3e, 3f).

METHODS

The **chemical composition of rocks** (Supplementary 1) was analyzed by XRF on a S8 Tiger (Bruker AXS GmbH, Germany) at the center for Collective Use of Research Equipment at the Voronezh State University (analyst E.Kh. Korish). Samples were prepared for their analysis for major components by melting 0.5 g of the powdered rock sample with 2g Li tetraborate and 2 g metaborate in a muffle furnace and the subsequent casting of glassy pellets. The spectrometer was calibrated and the quality of the analysis was controlled using certified state reference standard samples for the chemical composition of rocks: GSO №8871-2007, GSO № 3333-85, and GSO № 3191-85. The analysis was accurate to 1–2 relative % for concentrations

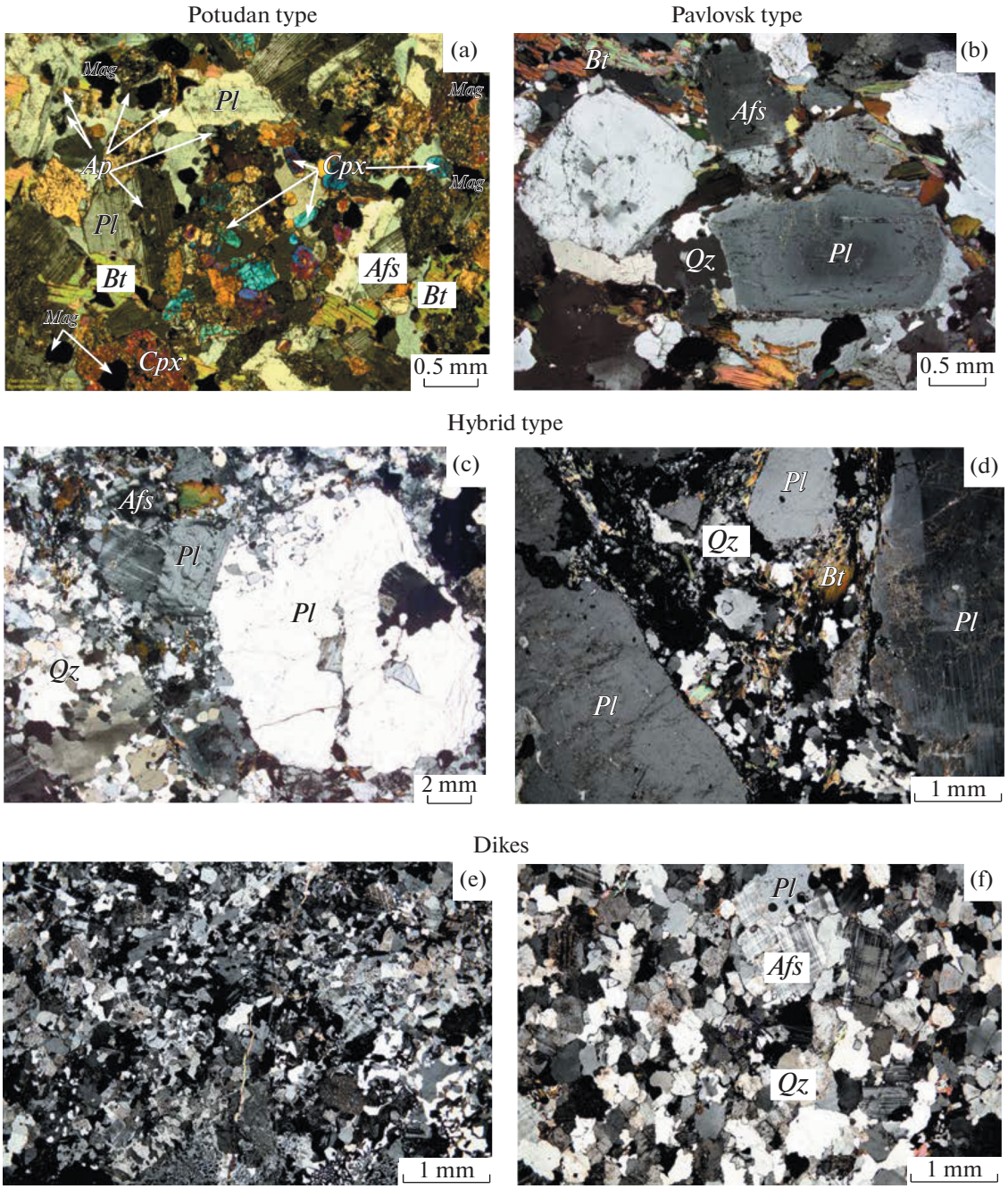

Fig. 3. Microphotographs of thin sections of granitoids of the Khokhol–Repyevka batholith: (a) Potudan type; (b) Pavlovsk type, (c, d) hybrid type; (e, f) dikes. Mineral symbols (Whitney and Evans, 2010): *Pl*—plagioclase, *Qz*—quartz, *Afs*—alkali feldspar, *Cpx*—clinopyroxene, *Bt*—biotite, *Mag*—magnetite.

higher than 1–5 wt % and no higher than 5 relative % at concentrations lower than 0.5 wt %.

Concentrations of trace elements and REE (Supplementary 1) were determined by ICP-MS at a laboratory of Karpinsky Russian Geological Research Institute of Geology (VSEGEI), in St. Petersburg (analysts V.A. Shishlov and V.L. Kudryashov). The samples were preparatorily decomposed by acids in either closed or open systems. The standard was an in-laboratory certified rock sample, which was decomposed by the same technique as the samples to be analyzed. The detection limits were 005–0.01 ppm for elements of intermediate to high atomic weight (U, Th, REE, etc.) and up to 0.01–3 ppm for light elements (Ba, Rb, etc.).

Sm–Nd isotope analysis was carried out on a TRITON TI thermal-ionization multicollector mass spectrometer, in static mode, at a laboratory of VSEGEI. The powdered samples (100–150 mg) were

spiked with a ^{149}Sm–^{150}Nd tracer and then decomposed by mixture of HCl + HNO_3 + HF at a temperature of 110°C. For the purposes of isotope analysis, Sm and Nd were separated in two stages: (1) by cation-exchange chromatography with AG1-X8 resin to separate REE from the mass of the rocks and minerals and (2) by extraction chromatography with the use of HDEHP solvent on Teflon. The correction for isotope fractionation was introduced by normalizing the measured values to $^{146}Nd/^{144}Nd = 0.7219$. The correction for the systematic error of the tool was done by normalizing to $^{143}Nd/^{144}Nd = 0.511860$ in the La Jolla Nd standard. The blanks were usually 0.03–0.2 ng for Sm and 0.1–0.5 ng for Nd. The concentrations of Sm and Nd were measured accurate to ±0.5%, and the isotope ratios were determined accurate to ±0.5% for $^{147}Sm/^{144}Nd$ and ±0.005% for $^{143}Nd/^{144}Nd$ (2σ).

The parameter $\varepsilon_{Nd}(t)$ was calculated using isotope ratios for CHUR: $^{143}Nd/^{144}Nd = 0.512638$ and $^{147}Sm/^{144}Nd = 0.1967$ (Jacobsen and Wasserburg, 1984). The model age (t_{DM}) values were calculated using the following isotope ratios for the depleted mantle: $^{143}Nd/^{144}Nd = 0.513151$ and $^{147}Sm/^{144}Nd = 0.2136$ (Goldstein and Jacobsen, 1988).

The **Rb–Sr isotope analysis** was done in six samples at the Institute of Precambrian Geology and Geochronology, Russian Academy of Sciences, in St. Petersburg. Three of the samples were granite of the Pavlovsk type, one was Potudan-type granite, one was hybrid granite, and another one was taken from a leucogranite dike. The powdered samples were decomposed by mixture of concentrated acids in the proportions HF : HNO_3 : $HClO_4$ = 5 : 1 : 1 in Savillex® closed fluoroplastic vessels at 120°C for 24 h. Before their decomposition, the samples were spiked with mixed ^{85}Rb–^{84}Sr tracers (Gorokhov et al., 2007, 2019). Upon the evaporation of the solution, the samples were treated by mixture of concentrated HCl : HNO_3 for 24 h to get rid of fluorides. After this, the solutions were evaporated and transformed to chloride forms. Rb, Sr, and REE were extracted on BioRad® ion-exchange resin. Rb and Sr were separated from total REE on Ln-Resin (Eichrom®) ion-exchange resin by the method in (Gorokhov et al., 2007, 2019). The blanks were 0.05 ng for Rb, 0.2 ng for Sr, and 0.05 ng for REE.

Sr isotopic composition was determined on a Triton TI multicollector mass spectrometer. Concentrations of Rb and Sr and the $^{87}Rb/^{86}Sr$ and $^{87}Sr/^{86}Sr$ ratios were determined by isotope dilution. The reproducibility of the determined Rb and Sr concentrations was evaluated by multiple replicate analyses of the BCR-1 standard and was ±0.5%. The analysis of the standard sample (six analyses) yielded the following results: [Sr] = 336.7 ppm, [Rb] = 47.46 ppm, $^{87}Rb/^{86}Sr = 0.4062$, and $^{87}Sr/^{86}Sr = 0.705036 \pm 0.000022$. The reproducibility of the isotope analyses was controlled by replicate analyses of the SRM-987 Sr standard. During the analytical session, the $^{87}Sr/^{86}Sr$ ratio of the SRM-987 standard was 0.710274 ± 0.000006 (2σ, $n = 11$). The isotopic composition of Sr was normalized to $^{88}Sr/^{86}Sr = 8.37521$.

Thermodynamic numerical simulations of the magmatic mineral-forming processes was applied to evaluate parameters under which the rocks were formed and was based on the minimization of the Gibbs energy. We studied the processes of fractional crystallization (FC) and fractional crystallization with assimilation (AFC) of the rocks and the probability of the mixing of two magmas (RFC, recharge fractional crystallization). The numerical simulations were carried out by the MCS program modulus (Bohrson et al., 2014) of the MELTS software (Ghiorso and Sack, 1995; Asimow and Ghiorso, 1998).

The MELTS program package uses a model of twelve-component silicate melt in the system SiO_2–TiO_2–Al_2O_3–Fe_2O_3–Cr_2O_3–FeO–MgO–CaO–Na_2O–K_2O–P_2O_5–H_2O. This model operates using the thermodynamic properties of magmatic rock-forming minerals: olivine (Mg, Fe^{2+}, Ca), pyroxenes (Na, Mg, Fe^{2+}, Ca)^{M2} (Mg, Fe^{2+}, Ti, Fe^{3+}, Al)^{M1} (Fe^{3+}, Al, Si)$_2^{TET}O_6$, feldspars (Na, Ca, K), spinel (Mg, Fe^{2+}) (Fe^{3+}, Al, $Cr)_2O_4$–(Mg, $Fe^{2+})_2$ TiO_4, and rhombohedral oxides (Fe^{2+}, Mg, Mn^{2+}) TiO_3–Fe_2O_3.

The MELTS program package has been calibrated by its authors on more than 2500 experimentally determined compositions of silicate melts that coexisted with the mineral association apatite ± feldspar ± leucite ± olivine ± pyroxene ± quartz ± rhombohedral oxides ± spinel ± whitlockite ± water at specified temperature, pressure, and oxygen fugacity. The model is applicable to natural magmatic systems (both hydrous and anhydrous) ranging in composition from potassic ankaratrite to rhyolite within the temperature range of (T) 900–1700° C and pressures (p) up to 4 GPa.

The partition coefficients were compiled from the EarthRef database (https://kdd.earthref.org/KdD/) and are presented in Supplementary 2.

GEOCHEMISTRY AND ISOTOPE GEOCHEMISTRY OF ROCK OF THE KHOKHOL–REPYEVKA BATHOLITH

The composition points of rocks of the Khokhol–Repyevka batholith plot in the TAS diagram within the fields of rocks ranging from monzogabbro to granite (Fig. 4). Representative chemical analyses of the rocks are presented in Supplementary 1, which also shows, for comparison, published petrochemical data on the granites of the Liski complex in the central part of the Don terrane (Terentiev, 2016).

Note that the highest $Na_2O + K_2O$ concentrations were found in the mafic rocks of the Potudan type and more felsic types of the Pavlovsk and hybrid types,

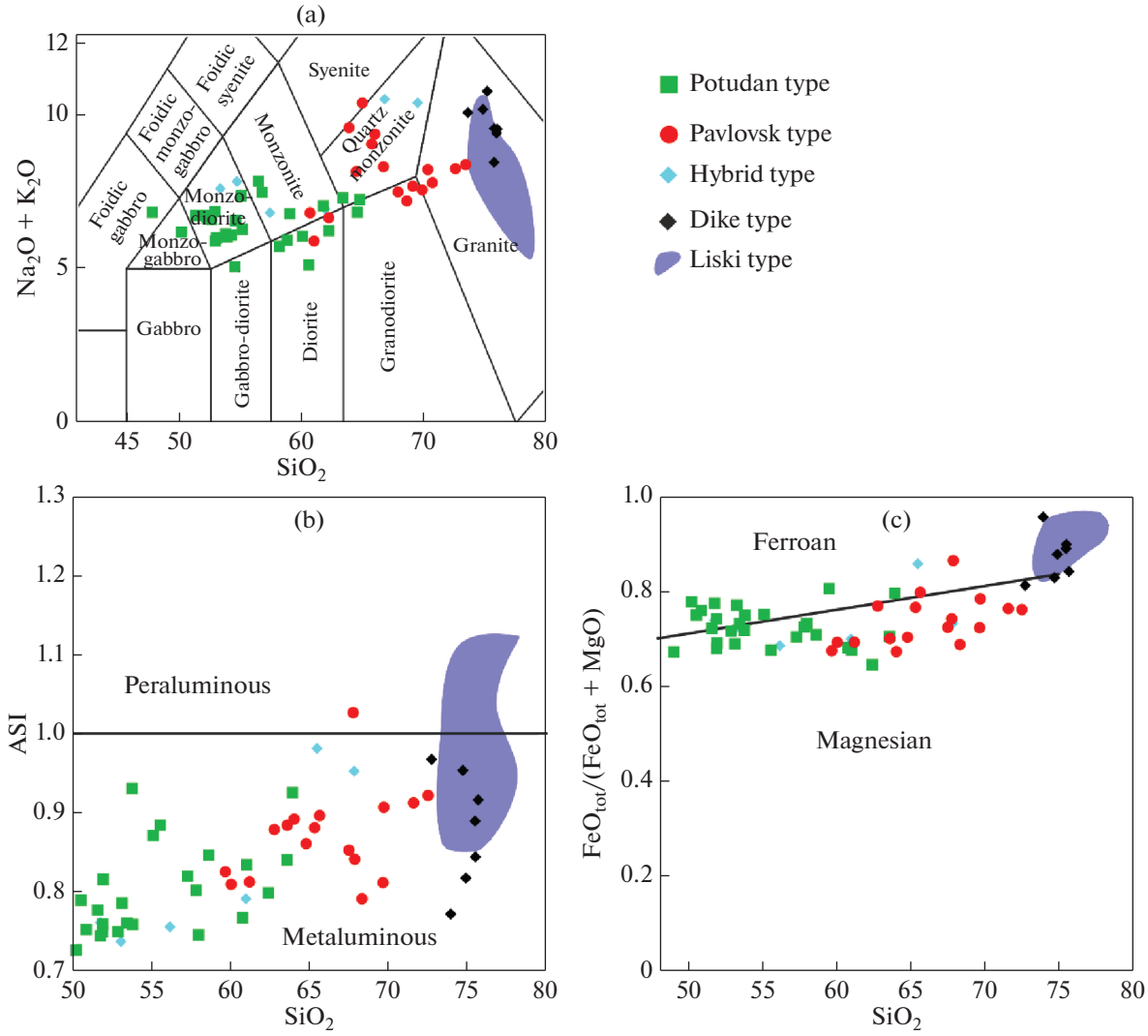

Fig. 4. Classification diagrams for rocks of the Khokhol–Repyevka batholith: (a) TAS diagram (Middlemost, 1994), (b) SiO_2–ASI (alumina saturation index) diagram, (c) SiO_2–$FeO_{tot}/(FeO_{tot} + MgO)$ diagram (Frost et al., 2001). The fields of Liski-type granites are according to (Terentiev, 2016). The diagrams show major-component compositions normalized to 100% anhydrous residue.

which are classified with quartz monzonite, as well as in some samples from the dike suite and Liski-type rocks that plot within the granite field (Fig. 4a).

Most rocks of the Khokhol–Repyevka batholith are metaluminous according to their A/CNK = Al/(Ca + Na + K) < 1.1. The Liski-type granites are metaluminous to peraluminous (Fig. 4b). According to their Fe# (Frost et al., 2001), more mafic Potudan-type granites, some granites of the dike suite, and the Liski-type granites belong to the ferroan series, whereas the Pavlovsk-type granites mostly affiliate with the magnesian series (Fig. 4c).

Mineralogical features of the Potudan-type granites (abundant Fe–Ti oxides and clinopyroxene) correspond to their chemical composition. The monzonitoids are richer in TiO_2 (0.5–2.3, here and below in wt %), MgO (1.5–6.1%), FeO_{tot} (6.1–13.9%), and CaO (4–8.2%) than the quartz monzonites, syenites, and granites. The Pavlovsk-type granites contain slightly lower concentrations of TiO_2 (0.3–1.4%), MgO (0.5–3.5%), FeO_{tot} (1.8–8.7%), and CaO (2.2–5.9%) than in the Potudan-type rocks because of the strong differentiation of the compositions. The dike leucogranites contain comparable concentrations of TiO_2 (0.08–0.30%), MgO (0.06–0.51%), FeO_{tot} (1.4–2.4%), and CaO (0.4–1.5%) with those in the Liski-type rocks: TiO_2 (0.11–0.32%), MgO (0.07–0.39%), FeO_{tot} (1.3–2.8%), and CaO (1.0–1.4%). The hybrid rocks also show scatters in concentrations of TiO_2 (0.02–1.82%), MgO (0.7–3.8%), FeO_{tot} (2.3–10.7%), and CaO (1.1–7.0%).

Systematic negative correlations were found between concentrations of TiO_2, CaO, MgO, and FeO_{tot} and those of SiO_2, and a notable feature of the

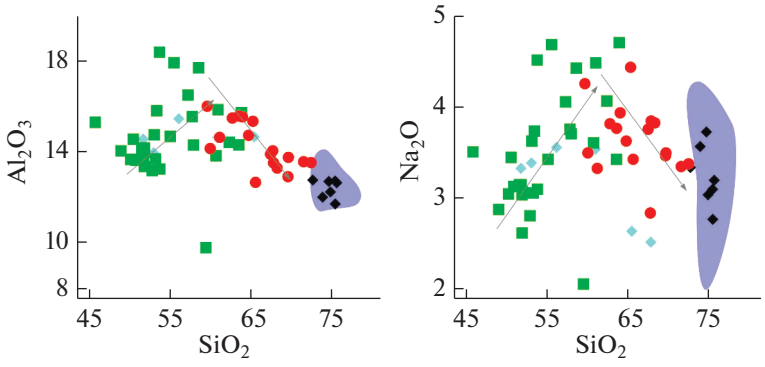

Fig. 5. Al_2O_3 vs. SiO_2 and Na_2O vs. SiO_2 diagrams for rocks of the Khokhol–Repyevka batholith. Lines show composition trends of the rocks of different type. See Fig. 4 for symbol explanations.

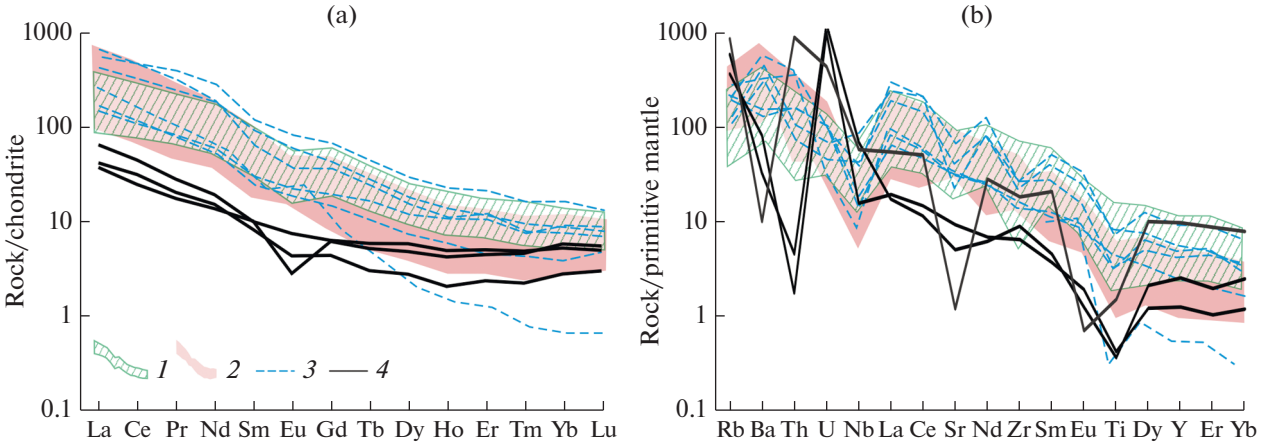

Fig. 6. (a) Chondrite-normalized and (b) primitive mantle-normalized (Sun and McDonough, 1989) multielemental patterns of rocks of the Khokhol–Repyevka batholith. (*1*) Field of the Potudan-type rocks, (*2*) field of the Pavlovsk-type rocks, (*3*) field of hybrid-type rocks, (*4*) dikes.

rocks is a change in the Na_2O and Al_2O_3 concentrations in rocks with SiO_2 concentrations of about 60% (Fig. 5).

The **rocks of the Pavlovsk and Potudan types** are characterized by fractionated distributions of REE with $(La/Yb)_N$ = 12.0–73.2, $(Gd/Yb)_N$ = 3.1–4.2 (Table 1) and weak Eu anomalies, Eu/Eu* = 0.67–0.76 (Fig. 6). The primitive mantle-normalized trace-element patterns of the rocks show enrichment in Rb, Ba, U, and LREE at depletion in Nb, Zr, Ti, and Th.

The chondrite-normalized multielemental patterns of the **hybrid rocks** are close to those of more felsic types of the Pavlovsk granites, $(La/Yb)_N$ = 33–300 and $(Gd/Yb)_N$ = 4–11, show no Eu anomalies or positive Eu anomalies in silicic derivatives (Eu/Eu*=0.7–1.6) (Table 1, Fig. 6 a). The primitive mantle-normalized trace-element patterns of the rocks display strong enrichment in Rb, Ba, Th, and U and depletion in Nb, Zr, and Ti (Fig. 6b).

The leucogranite dikes are characterized by moderate REE fractionation with $(La/Yb)_N$ = 6.5–15.2 and $(Gd/Yb)_N$ = 1.1–1.6, with negative Eu anomalies, Eu/Eu*= 0.4–0.96. The rocks of this type are strongly enriched in Rb and U and have Nb–Zr–Ti minimum (Fig. 6).

Sm–Nd and Rb–Sr Systems of the Rocks

The **monzonitoids of the Potudan type** in the Potudan pluton itself have $\varepsilon_{Nd}(2.06)$ = –3.1 to –3.7 and a model age of $t_{Nd}(DM)$ = 2.7 Ga. Analogous rocks from a massif in the northern part of the Khokhol–Repyevka batholith (this massifs was drilled through by Borehole 7577) (Fig. 2) yielded $\varepsilon_{Nd}(2.07)$ = –1.7 and a model age of $t_{Nd}(DM)$ = 2.6 Ga. The initial isotope ratios $^{87}Sr/^{86}Sr(i)$ of three samples are 0.70381 to 0.70910 (Table 1).

The **Pavlovsk-type granitoids** are characterized by $\varepsilon_{Nd}(2.08)$ = +0.2 to –4.2 and $t_{Nd}(DM)$ = 2.4–2.8 Ga

Table 1. Sm–Nd and Rb–Sr isotope date on Paleoproterozoic rocks of the Khokhol–Repyevka batholith

Type	Sample	Rock	Sm ppm	Nd ppm	$^{147}Sm/^{144}Nd$	$^{143}Nd/^{144}Nd$	t, * Ma	$\varepsilon_{Nd}(t)$	$t_{Nd(DM1)}$, Ma	Rb ppm	Sr ppm	$^{87}Rb/^{86}Sr$	$^{87}Sr/^{86}Sr$ measure.	$^{87}Sr/^{86}Sr$ init.
Potudan	6418/66	*Qz MGb*	15.67	94.75	0.1000	0.511136	2056	−3.8	2687	87.3	801	0.31541	0.71845	0.709102
	8003/365	*Qz MGD*	9.053	53.07	0.1031	0.511212	2056	−3.1	2658	69.0	983	0.20294	0.70983	0.703813
	7577/170	*Qz MGD*	10.93	56.25	0.1175	0.511472	2067	−1.7	2491	57	3144	0.05264	0.70759	0.706016
Pavlovsk	7578/155	*Gd*	9.985	74.32	0.0812	0.510975	2073	−1.7	2491	96.5	711	0.39240	0.71507	0.703351
	K-85/105***	*Qz MDi*	2.70	16.85	0.0969	0.511288	2077	0.3	2421	–	–	–	–	–
	K-50/236.8***	*Mz*	10.76	59.97	0.1085	0.511223	2066	−4.2	2778	–	–	–	–	–
	K-10/127**	*Gd*	2.75	15.45	0.1076	0.51136	2078	−1.2	2571	158.3	580.9	0.78839	0.72661	0.70300
	K-106/130**	*Gd*	2.10	13.05	0.0971	0.51126	2078	−0.3	2467	112.6	480.9	0.67751	0.72224	0.70195
	K-236/1**	*Gd*	4.60	28.84	0.0964	0.51121	2078	−1.1	2514	132.5	992.3	0.38637	0.71422	0.70264
Hybrid	7576/200	*Gd*	3.786	34.04	0.0672	0.510426	2068	−8.8	2819	141.0	695	0.58853	0.72352	0.705964
Dikes	6435/77	*Gr*	0.443	4.912	0.0545	0.510300	2073	−7.8	2715	152	145	3.04490	0.79274	0.701777
	188/д@	*Gr*	1.853	11.37	0.0985	0.511103	2077	−3.8	2695	–	–	–	–	–

The values of $\varepsilon_{Nd}(t)$ and the $^{87}Sr/^{86}Sr$ ratios were calculated using the known U–Pb zircon age (*) for each rock type. The isotope data are from ** (Shchipansky et al., 2007); *** (Terentiev et. al., 2020).

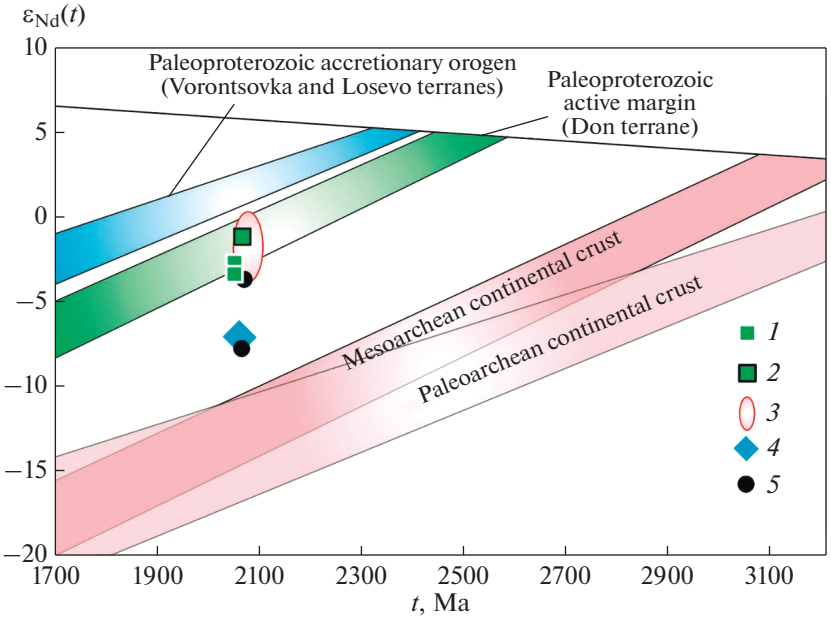

Fig. 7. t (Ma)–ε_{Nd}(t) diagram for rocks of the Khokhol–Repyevka batholith. (*1*, *2*) Potudan-type rocks: (*1*) northern massif (sample 7577), (*2*) Potudan pluton; (*3*) Pavlovsk-type (Terentiev et al., 2020); (*4*) hybrid type; (*5*) dike rocks. Fields show the Nd isotopic composition evolution of the Paleoproterozoic crust of terranes in the Volga–Don orogen and Archean crust of the Kursk blocks (Terentiev et al., 2017; Savko et al., 2018).

(Terentiev et al., 2020). Our sample of the Pavlovsk granodiorite (sample 7578/155) shows higher $\varepsilon_{Nd}(2.07) = -1.7$ than that of the Potudan-type quartz monzogabbro with $\varepsilon_{Nd}(2.06) = -3.7$. The initial isotope ratio of this sample $^{87}Sr/^{86}Sr(i) = 0.70335$ (Table 1) is close to the range of 0.70269–0.70309 reported for granitoids from the Pavlovsk batholith (Shchipansky et al., 2007).

The **hybrid rocks** are characterized by a low radiogenic Nd isotope composition with $\varepsilon_{Nd}(2.07) = -8.7$ and a model age of $t_{Nd}(DM) = 2.8$ Ga, which indicates that the source contained much ancient crustal material. The initial isotope ratio $^{87}Sr/^{86}Sr(i) = 0.70596$ (Table 1).

The **dike leucogranites** show broad variations in the isotope ratios. For example, sample 188/d yielded $\varepsilon_{Nd}(2.08) = -3.8$ and $t_{Nd}(DM) = 2.7$ Ga, which are close to those of the Pavlovsk-type rocks. Sample 6435/77 from dike has $\varepsilon_{Nd}(2.07) = -7.8$, $t_{Nd}(DM) = 2.7$ Ga, and the highest $^{87}Rb/^{86}Sr$ ratio at the lowest initial $^{87}Sr/^{86}Sr(i) = 0.70177$ (Table 1). The low ε_{Nd} values (–7.8) and the high Rb concentrations may mean that the leucogranites were contaminated by crustal material. This may perhaps occur later in the geological history and resulted in an erroneous initial $^{87}Sr/^{86}Sr$ ratio. No other samples with such Rb–Sr characteristics have been found (at least so far) in VDO, and hence, this sample was rejected from all other considerations.

In the age–εNd(t) diagram (Fig. 7), the rocks fall within the field of the Nd isotope composition evolution of the Paleoproterozoic crust of the Don terrane, except only the hybrid rocks and those of some dikes, whose composition points plot between the field of the Paleoproterozoic crust of the Don terrane and the Archean continental crust of the Kursk block.

THERMODYNAMIC MODELING OF THE FRACTIONAL CRYSTALLIZATION, ASSIMILATION, AND MAGMA RECHARGE

Petrakova et al. (2022b) conducted numerical thermodynamic simulations of the fractional crystallization (FC) by means of varying additional criteria (*P–T* parameters, water content, and oxygen fugacity) to confirm the differentiation model for the Potudan and Pavlovsk rocks along different evolution branches, which indicates that the melts of the two types were derived from different sources. With regard to the newly acquired isotope data, herein we tested the models of contamination (AFC) and mixing (Recharge) to explain the origin of a wider rock spectrum composing the Khokhol–Repyevka batholith.

External parameters for modeling the FC process were chosen using the results of mineral thermobarometry. The pressure in the magma chamber was evaluated by the Al-in-Hbl geobarometer at 3 kbar (Petrakova and Terentiev, 2018). The simulations were carried out to a temperature of 850°C to avoid uncertainties related to simulations with hydrous minerals,

whose thermodynamic properties are still poorly determined. Water content in the magma was evaluated from the composition of the amphiboles (Ridolfi and Renzulli, 2010): it was 3–4 wt % for the magmas of the Potudan-type granites, and 4.5–6 wt % for the Pavlovsk-type ones. To analyze the AFC process, the temperature of the wall rocks was assumed to be 400°C with regard to the geothermal gradient in the upper–middle crust (3-4 kbar) (Koronovskii and Yasamanov, 2012). The melt percolation limit (the percentage of the anatectic melt) was assumed to be 10 vol %. The wall rocks in the AFC model were assumed to originally contain 1 and 3 wt % H_2O. To test the recharge model, a new magma portion was introduced at 100°C intervals of the starting magma fractionation, with the addition of 10 to 200 g new portions of magma of other composition.

In the models with contamination and mixing with felsic melt, the starting composition was assumed to be that of the least evolved monzogabbro of the Potudan type (sample 8003/255). Considering that the rocks of the batholith occur in contact with Archean rocks of the Kursk block, the possible contaminant in the AFC model was assumed to be TTG gneiss form this block (sample 7516, Shchipansky et al., 2007). The models of mixing (Recharge) were simulated using the composition of Pavlovsk-type granite and the average composition of experimentally obtained partial melt derived from rocks of the Kursk block (mixture of metapelite and TTG; Savko et al., 2021). All used compositions are listed in Table 2.

FC model. The early crystallization of the Potudan-type melt is marked by the fractionation of olivine and magnetite from the melt, and hence, the melt enriches in alkalis. The early crystallization of the Pavlovsk-type melt involves clinopyroxene and plagioclase fractionation (see Petrakova et al., 2022b for detail).

These concentrations of Fe–Mg and K–Na components in the melts at high temperatures (~1200°C) still allow anhydrous minerals (*Ol* and *Cpx*) to crystallize from these melts, but these minerals cease to crystallize at 50–100°C lower temperatures and give way to the assemblages found in the rocks: *Pl* + *Cpx* + *Spl*. Once a temperature of 900°C is reached by the melt and water content in it reaches 4.5% (or higher), hydrous minerals (*Bt*) start to crystallize, and the late crystallization of alkali feldspar is thought to begin.

The partial fractionation of *Ol* + *Spl* in the Potudan-type melt occurs in all of the models (Table 3). The absence of olivine-bearing rocks among those of the Potudan type may be explained by the early fractionation of this mineral from the melt. In this situation, olivine-bearing rocks may have been formed in intermediate chambers or at deeper levels in the batholith that were not reached by boreholes.

AFC model. The addition of 10% partial melt derived from TTG to the Potudan-type magma results in an increase in the SiO_2 concentration (Fig. 8), a decrease in the Ca concentration in the plagioclase, and an increase in the percentage of fractionated alkali feldspar (Table 3).

The Nd isotope ratios decrease to 0.51109, and a deep Ti minimum is formed.

Recharge 1 model (with the addition of the Pavlovsk-type magma). We have tested models with different proportions of the added felsic melt to obtain the required composition range of the hybrid rocks. We have found out that the addition of a single portion of the melt was insufficient, and the most suitable model involved the addition of two portions of the felsic melt in the mass proportion of 1 : 2. The model and real compositions are compared in Fig. 8. The compositions are shifted toward the field of normal alkalinity and become notably enriched in Al_2O_3, as in the AFC model, which is most likely explained by *Spl* accumulation during early crystallization and the late crystallization of *Pl* (of calcic to intermediate composition) (Table 3).

The Nd isotope ratios decrease to 0.51104, and the REE patterns correspond to those of some of the hybrid rocks.

Recharge 2 model (with the addition of partial melts from TTG gneisses). In this model, we assumed the average composition of TTG gneiss from (Shchipansky et al., 2007), for which the composition of the derived granite melt (Table 2) was calculated using the Perplex software (Connolly, 1990). We have also calculated the average composition of partial melt derived from rocks of the Kursk block (TTG + metapelite) from Savko et al., 2021). All other parameters were as in the model Recharge 1. Both compositions yield similar model trajectories, and Fig. 8 shows the evolution of the composition of mixture of the Potudan-type melt and the average composition of partial melt from TTG + metapelite. This model does not yield drastic jumps in the Al_2O_3 concentration, which is explained by the early removal of *Spl* and the early crystallization of sodic *Pl* and *Opx* (Table 3).

The Nd isotope ratios significantly decrease to 0.51078. The REE patterns are as in some of the hybrid rocks.

DISCUSSION

Detailed petrographic–mineralogical observations on the crystallization sequences of minerals in rocks of the Pavlovsk and Potudan type have been discussed in (Petrakova and Terentiev, 2018; Petrakova et al., 2022a). It was pointed out that an increase in the SiO_2 concentration negatively correlates with the MgO, FeO, CaO, Cr, and Ni concentrations and reflects the early removal of pyroxene and magnetite. The negative correlations of TiO_2, P_2O_5, and Zr with SiO_2 indicate that accessory minerals containing these elements (zircon, apatite, and titanite) also early crystallized in the magmas. At the same time, no adequate attention

Table 2. Concentrations of major components (wt %) and trace elements (ppm) in the selected samples

Sample	Potudan type (original magma)	Pavlovsk type (Recharge 1)	TTG (AFC)	TTG melting Perplex simulation, 3 kbar	Experim. melting, 4 kbar* (Recharge 2)
Composition	sample 8003/255	average composition	sample 7516	average composition	average composition
SiO_2	49.05	74.68	70.62	80.79	72.39
TiO_2	2.01	0.21	0.32	–	0.43
Al_2O_3	14.09	12.39	14.59	8.33	13.70
Fe_2O_3(tot)	13.89	1.38	2.62	1.92	1.65
MnO	0.14	0.01	0.12	–	0.96
MgO	6.11	0.55	0.88	0.70	0.12
CaO	6.64	1.49	3.05	0.96	0.63
Na_2O	2.87	3.20	4.64	4.85	2.59
K_2O	3.27	5.18	3.03	2.45	5.86
P_2O_5	0.84	0.05	0.13	–	0.10
Total	98.91	99.14	100.00	100.00	98.43
Trace elements in ppm					
Rb	75.0	148.6	84.27	–	345.0
Sr	723.0	727.6	368	–	266.0
Y	24.1	15.8	4.57	–	21.8
Zr	56.3	166.4	199.3	–	42.4
Nb	27.0	15.5	4.0	–	36.2
Ba	1340	1787	1265	–	1300
La	67.50	56.57	54.67	–	62.70
Ce	135	111	99.95	–	98
Pr	16.30	12.68	10.33	–	9.80
Nd	60.7	45.8	34.26	–	36.0
Sm	10.40	7.26	4.63	–	7.70
Eu	2.36	1.68	0.58	–	4.27
Gd	8.01	5.05	2.55	–	6.61
Tb	0.99	0.64	0.26	–	0.98
Dy	5.09	3.21	1	–	5.31
Yb	1.65	1.32	0.28	–	2.12
Lu	0.26	0.19	0.05	–	0.39
Hf	2.29	5.93	5.09	–	1.10
Ta	1.38	0.94	0.17	–	1.38
Th	6.47	18.69	20.24	–	14.90
$^{143}Nd/^{144}Nd$	0.51114	0.51098	0.51033	0.51033	0.51033

* Average composition of experimental partial melt derived from mixture of TTG and metapelite of the Kursk block.

was paid to the atypical decreases in the concentrations of LILE, K_2O, and Na_2O with an increase in the SiO_2 concentrations in the rocks of the Potudan type (Figs. 4, 5). These concentrations usually increase with ongoing melt fractionation. The Pavlovsk-type granite series was originally more differentiated, and the concentrations of the oxides decrease as the SiO_2 concentration increases from 60 to 74%. Our modeling of the fractional crystallization to a level when hydrous minerals start to crystallize (850°C) shows that the probable reason for this may have been the accumulation of alumina-bearing minerals (*Spl* and *Pl*) and the subsequent decrease in the role of *Spl* (magnetite) and its later fractionation from the melt,

Table 3. Sequence of mineral fractionation in the model

FC (8003/255)	**AFC 3 kbar (TTG)**
1192°C: *Ol* 4.4	–
1127°C: *Ol* 4.7 + *Spl* 0.39	–
1057°C: *Ol* 8.13 + *Spl* 4.97	–
1052°C: *Cpx*1.1 + *Spl* 5.3	–
1022°C: *Cpx* 6.01 + *Spl* 6.98 + *Ap* 0.08	–
902°C: *Cpx* 15.08 + *Spl* 9.84 + *Ap* 0.78 + *Pl* 0.33 (An67)	–
857°C: *Spl* 10.06 + *Pl* 5.17 (An56) + *Bt* 0.03	–
787°C: *Spl* 11.35 + *Pl* 12.6 (An37) + *Bt* 0.54 + *Kfs* 0.82	–
→	752°C: *Spl* 11.8 + *Pl* 20.2 (An21) + *Bt* 0.66 + *Kfs* 15.3 + *Ap* 0.04
FC (8003/255)	**Recharge 1 (+ Pavlovsk type)**
1204°C: *Ol* 0.39	–
1129°C: *Ol* 5.8 + *Spl* 0.13	–
1099°C: *Ol* 7.4 + *Spl* 2.6	–
→	1031°C: *Opx* 1.69
–	936°C: *Opx* 11.64
–	931°C: *Cpx* 0.88
–	911°C: *Cpx* 4.30 + *Rhm-oxide* 0.36
–	896°C: *Spl* 1.22 + *Cpx* 6.10
–	846°C: *Spl* 3.49 + *Cpx* 9.97 + *Pl* 13.14 (An33)
–	871°C: *Spl* 2.23 + *Cpx* 8.89 + *Pl* 1.73 (An37)
FC (8003/255)	**Recharge 2 (+ melt from metapelite–TTG)**
1204°C: *Ol* 0.39	–
1129°C: *Ol* 5.8 + *Spl* 0.13	–
1099°C: *Ol* 7.4 + *Spl* 2.6	–
→	992°C: *Opx* 8.46
–	936°C: *Opx* 13.46 + *Pl* 27.1 (An19)
–	913°C: *Pl* 47.6 (An37) + *Opx* 16.1 + *Kfs* 0.3 + *Rhm-Oxide* 0.64
–	893°C: *Pl* 49 (An18) + *Opx* 18 + *Kfs* 30.3 + *Rhm-oxide* 2.04 + *Qz* 3.2
–	888°C: *Spl* 1.9 + *Pl* 51 (An19) + *Kfs* 39 + *Qz* 9.2
–	863°C: *Pl* 57 (An25) + *Kfs* 75 + *Qz* 29 + *Rhm-Oxide* 2.5

Mineral symbols specify which minerals crystallized from the melt at its fractionation, numerals are the relative masses (in g) of these minerals. The composition of plagioclase is specified in parentheses (as the percentage of the anorthite end member). *Rhm-Oxide* is rhombohedral oxides, (Fe^{2+}, Mg, Mn^{2+}) TiO_3–Fe_2O_3.

the beginning of crystallization of clinopyroxene, biotite, potassic feldspar, and hence, a decrease in Ca concentration in the plagioclase.

High Ba and Sr concentrations in rocks are usually thought to indicate that feldspars accumulated in the course of differentiation (White et al., 2009). However, the absence of positive Eu anomalies in the monzodiorites and monzonites, the occurrence of an Eu minimum in the more felsic derivatives, and the negative correlations of Ba and Sr with increasing SiO_2 are consistent with the interpretation that the felsic Potudan and Pavlovsk-type melts were not feldspar cumulates. Moreover, Ba and Sr concentrations in the monzonitoids are much higher than in the continental crust. For example, the Archean TTG gneisses of the Kursk block that occur in contact with the Don terrane contain 573–1265 ppm Ba

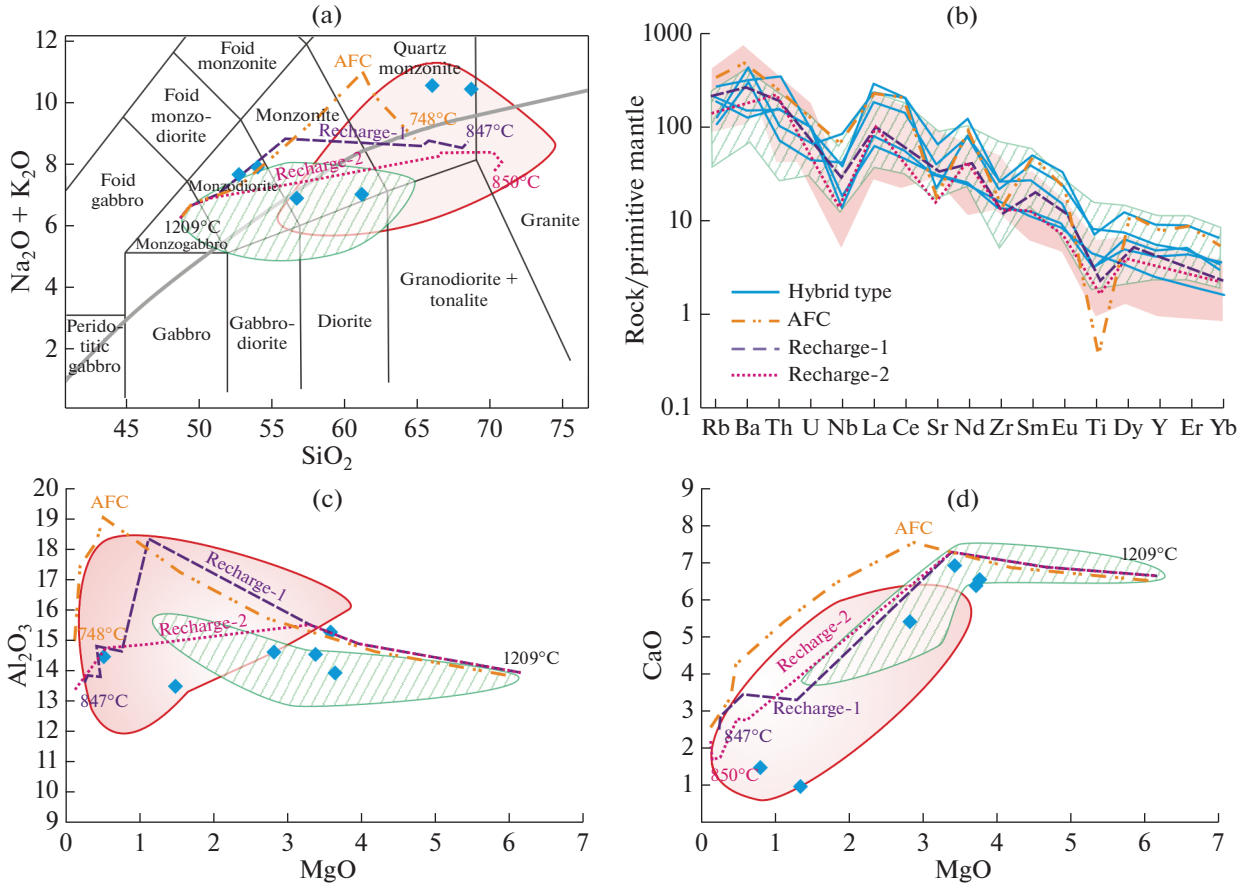

Fig. 8. Rock compositions (symbols are as in Fig. 4 and 6). Dashed lines: *AFC*—model composition at Potudan-type magma contamination with TTG gneisses at 3 kbar; *Recharge 1*—model composition at Potudan-type magma recharge (mixing) with two portions of Pavlovsk-type melt; *Recharge 2*—model composition at Potudan-type magma recharge two portions of felsic melt derived from mixture of Archean TTG and metapelite (Savko et al., 2021). The green hatched field is the composition of the Potudan-type rocks, the pink field is the composition of the Pavlovsk-type rocks, blue lozenges are hybrid rocks.

and 360–440 ppm Sr (Shchipansky et al., 2007), and this means that the contamination with/assimilation of TTG should have resulted in a decrease in the Ba and Sr concentrations but not their increase.

The Nd isotope composition of the hybrid granodiorite is more radiogenic than in the Potudan- and Pavlovsk-type rocks. This seems to mean that the Potudan-type mafic magmas mixed with some other felsic melt or may have been strongly contaminated by Archean crust.

The modeling of the AFC process of the Potudan-type monzogabbro with the Archean TTG gneisses shows a shift to the region of normal alkalinity and an insignificant increase in the SiO_2 concentration. Experimental data on the dehydration melting of high-Al tonalite and granodiorite at $P \leq 4$ kbar, $T > 900$°C, and water content of ≤ 4% (Patino Douce et al., 1997) demonstrate that felsic partial melts (peraluminous granite) can be derived in the upper crust. However, the modeling of the AFC process shows that the contamination/assimilation of hot water-saturated Potudan-type magmas at about 3 kbar should have occurred during later stages, when the starting melt has already acquired a granodiorite composition (SiO_2 = 60–63%). The specified contamination parameters imply that the wall rocks should have been heated to the temperature of melting and derivation of 10% anatectic melts, with their addition to the starting magma and further fractionation up to the final melt. The derivation of 10% melt from the host TTG gneisses at 3 kbar could have occurred if these rocks had been heated to 710°C, when the temperature of the original Potudan-type magma was close to the solidus (750°C) (Fig. 8).

Calculations with the MCS software (the *Traces & Isotopes* option) have shown changes in the isotope ratios for the AFC model at the addition of 10 wt % of the crustal partial melts derived from the TTG gneisses with $^{143}Nd/^{144}Nd$ = 0.51033 (sample 7516, Shchipansky et al., 2007) to the composition of the least differentiation sample (8003/255 with average $^{143}Nd/^{144}Nd$ = 0.51114), which resulted in a decrease

in the $^{143}Nd/^{144}Nd$ ratio to 0.51109. However, this is insufficient for obtaining $^{143}Nd/^{144}Nd = 0.51042$ of the hybrid granodiorite.

The mixing of two compositionally contrasting melts: Potudan-type mafic with $^{143}Nd/^{144}Nd = 0.51114$ and Pavlovsk-type felsic with $^{143}Nd/^{144}Nd = 0.51098$ yields a model composition reasonably well consistent with the composition of some of the hybrid rock samples in terms of proportions of major components and trace elements (Fig. 8). The Nd isotope ratio in the final product in this model (Recharge 1) is $^{143}Nd/^{144}Nd = 0.51104$, which means that, hypothetically, such mixing could have produced some of the hybrid rocks.

The results of Perplex thermodynamic modeling of TTG melting (Table 2) and experimental data on the melting of Archean TTG shows that high-K melt can be generated under such conditions (Watkins et al., 2007). Some of the hybrid and dike rock contain ≥2% K_2O, which led to the conclusion that the recycling of ancient crust that consisted of TTG alone is insufficient to generate high-K melts, which can be produced if the magma-generation region contains more fertile crustal rocks and/or strongly enriched mantle sources (Watkins et al., 2007). Melt of A-type granite was recently experimentally obtained (Savko et al., 2021) by 20% dehydration melting of metapelite + TTG mixture under a pressure no higher than 4 kbar and temperature of 950°C. The average composition of the partial melts thus obtained is more potassic and suitable for testing the Recharge model (Table 3).

As follows from the modeling result with regard to data on the experimental melting, the additional felsic melt required to produce some of the hybrid and dike rocks might have been melts derived from Archean rocks of the Kursk block (metapelite–TTG).

The close spatiotemporal relations of the studied granitoids of the Khokhol–Repyevka batholith suggest their possible genetic relations. Geochemical and isotope data provide grounds for distinguishing the following two groups of the dike leucogranites. (1) Leucogranites with $\varepsilon_{Nd}(t) = -1.7$ to -4.6 and fractionated patterns of HREE (Gd_N/Yb_N=2.1–3.8). These rocks might have been formed by the deep differentiation of the Pavlovsk-type magma that had been produced in equilibrium with garnet-bearing residue. Such conditions might have occurred if monzodiorite–granodiorite melt was generated by melting mafic rocks in the lower crust under pressures of 10–15 kbar (Topuz et al., 2005; Qian and Hermann, 2013; Gao, 2016) (Fig. 10). (2) Rocks with not as strongly fractionated HREE patterns (Gd_N/Yb_N = 1.1–1.6), a feature that may have resulted from the melting of felsic rocks in the middle crust, with plagioclase in the residue, under a pressure of about 5 kbar (Gao, 2016).

One of the reasons for crust melting at different depth levels is sometimes thought to be the involvement of basalt magmas (Huppert and Sparks, 1988; Annen et al., 2008; Gao, 2016). The probable involvement of mafic melts in processes that produced the granitoids follows from that monzogabbro occurs among the Potudan-type rocks. Heat from hot mafic intrusions in the central part of the Don terrane could have induced the melting of rocks of the Archean basement of the Kursk block, which is heterogeneous and consists, in the study area, of recycled TTG gneisses of the Rossosh block (Savko et al., 2014; Mints et al., 2017). The Liski granite–leucogranite complex occurs nearby in the central part of the Don terrane, south of the Potudan pluton. The Liski leucogranites show features characteristic of A-type granites: high SiO_2, $K_2O + Na_2O$, and F concentrations, high FeO*/MgO and TiO_2/MgO ratios, low CaO and MgO concentrations, high liquidus temperatures (870 ± 18°C), and specific sets of accessory minerals, including xenotime, tantalates–niobates, and fluorite (Terentiev, 2016). The age of the Liski leucogranites is 2064 ± 14 Ma (Terentiev, 2016), i.e., they are almost exactly coeval with the Potudan complex, whose age is 2056–2068 Ma

Liski-type magma may have served as an additional source for the hybrid rocks and some of the dikes, as is demonstrated in the triangle plot of the sources in Fig. 9.

If the magmatic activity was intense and two or more magmas occurred simultaneously, these magmas could mix with one another. This mixing should result in systematic shifts in the geochemical and isotope-geochemical parameters of the rocks, and this is also confirmed by results of thermodynamic modeling on the basis of the geochemistry and isotope composition of the real rocks. For example, changes in the Nd isotope composition, either smoother (0.51114–0.51104, if portions of Pavlovsk-type magma were added, model Recharge 1) or sharper (with the addition of Archean TTG, Recharge 2), indicate that not only mafic but also felsic melts could mix. The latter might have been of crustal provenance or be produced by the evolution of magmas derived within the mantle. Magmas of the two types could interact at high temperatures that decreased the difference between their viscosities.

The Nd–Sr isotope data indicate (Fig. 10) that the Khokhol–Repyevka batholith was contributed by at least three components: (1) lower mantle (or buried oceanic crust) of predominantly mafic composition and/or enriched mantle metasomatized in the Proterozoic, whose involvement is "recorded" in the composition of the Pavlovsk-type granitoids; (2) an enriched mantle source, which was likely subcontinental lithospheric mantle, which may have been metasomatized during an earlier stage of the regional geological evolution, which is typical of the Potudan-type monzonitoids; and (3) Archean crust, which was dominated by TTG and metasediments and was affected by melting.

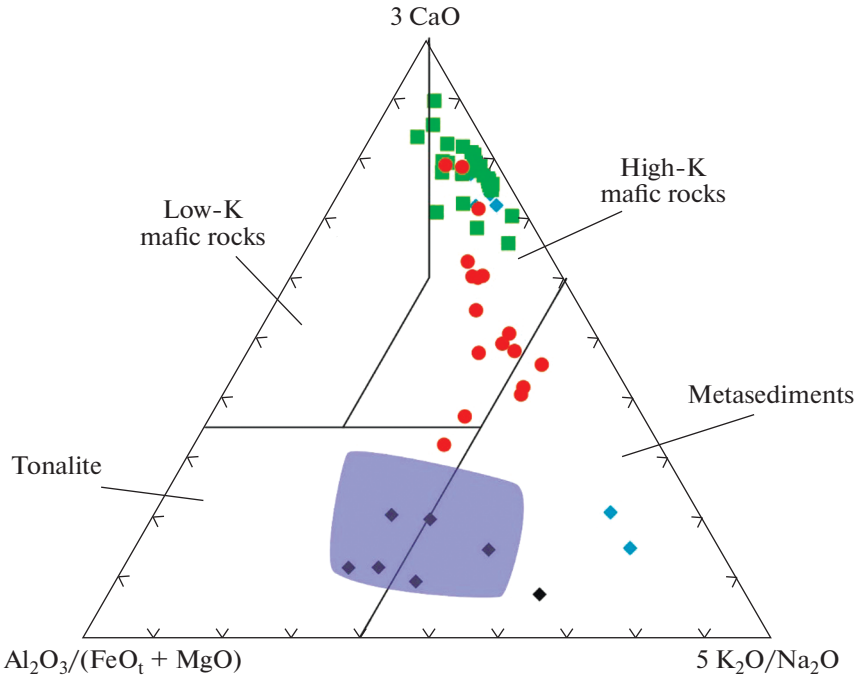

Fig. 9. $Al_2O_3/(FeO_t + MgO)–3CaO–5K_2O/Na_2O$ triangular plot for the sources (according to Laurent et al., 2014). See Fig. 4 for symbol explanations.

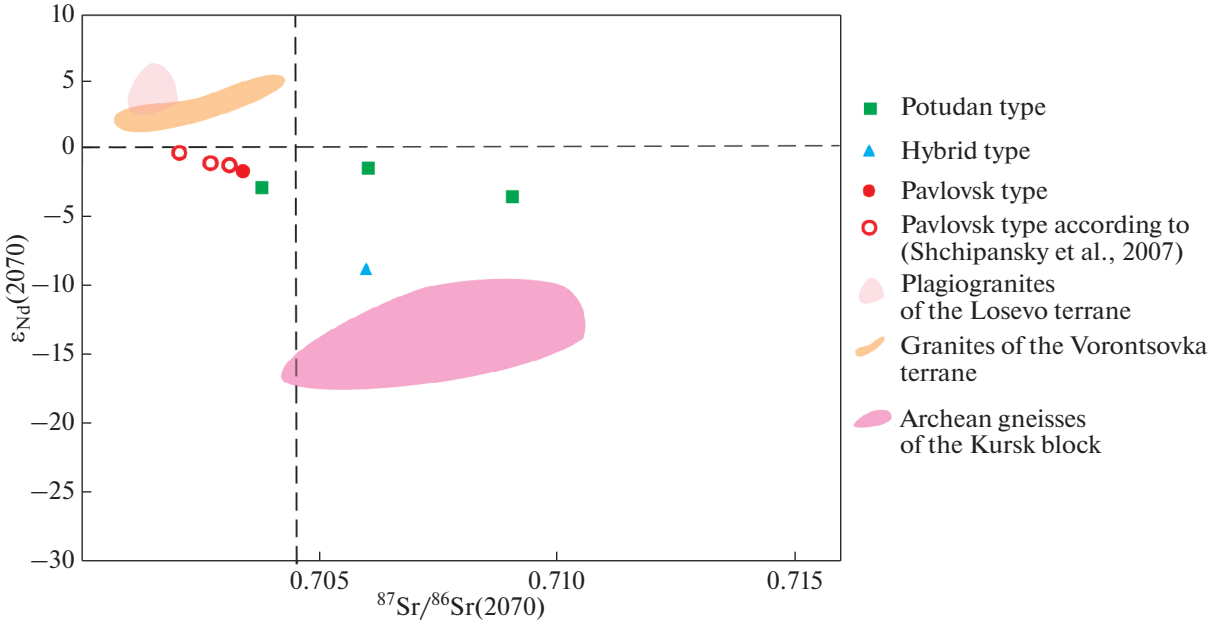

Fig. 10. $^{87}Sr/^{86}Sr$ (i)–ε_{Nd} diagram for rocks of the Khokhol–Repyevka batholith and granitoid complexes in adjacent terranes. For comparison, the diagram shows the compositions of the Archean TTG gneisses of the Oboyan complex of the Kursk block recalculated to an age of 2070 Ma. The isotopic composition of the granites of the Losevo and Vorontsovka terranes and Archean rocks are given according to (Shchipansky et al., 2007).

The shift in the Nd isotope composition toward more radiogenic values in the Potudan-type diorites in the northern massifs of the batholith (drilled by Borehole 7577), as well as their Fe-poorer composition than the petrotypical rocks of the Potudan massif, suggests that Pavlovsk-type magma with a more radiogenic Nd isotope composition might have been involved in the processes. The leucogranite dikes and some of the

hybrid rocks were contributed by partial melts derived from the Archean crust of the Kursk block.

It is also worth mentioning the enriched nature of the mantle source of the Potudan rocks, whose analogues were not found in the area. Isotope data on the granitoids of the neighboring Losevo and Vorontsovka terranes (Shchipansky et al., 2007) indicate that all composition points of all granitoids and host rocks plot onto the mantle sequence line. The generation of enriched mantle sources as a results of Paleoproterozoic subduction and collision processes with the involvement of crustal material also follows from the high Th/Yb–Ta/Yb ratios (Supplementary 1; illustrations in Petrakova et al., 2022a) for all magmatic complexes of VDO with age within the range of 2080–2050 Ma. However, some of alkaline basalts that have low $^{143}Nd/^{144}Nd$ and high $^{86}Sr/^{87}Sr$ were formed by the melting of mantle rocks enriched in LILE billions of years ago (Guo et al., 2006; Ariskin et al., 2015).

Such relations to the enriched lithospheric mantle were found in Paleoproterozoic rocks in the southwestern Siberian craton. Experimental data on the melting of various protoliths and numerical simulations indicate that the monzodiorites–granodiorites of the Toisuk and granodiorites of the Nizhnii Kitoi massifs in the Sharyzhalgai basement inlier were formed via the differentiation/melting of a mantle source whose Ba and Sr concentrations were similar to those of intraplate continental basalts. The Hf isotope composition of the zircon and Nd isotope composition of the melanocratic granitoids of the Toisuk (ε_{Hf} = 6.0 to −10.7 and ε_{Nd} = −5.3 to −10.2) and Nizhnii Kitoi (ε_{Hf} = −5.0 to −8.1, ε_{Nd} −4.0 and −5.1) massifs indicate that their mafic sources were derived from enriched lithospheric mantle that had been produced by Neoarchean subduction processes at 2.7 Ga (Turkina and Kapitonov, 2019).

Some researchers are prone to believe (Guo et al., 2006; Pilet et al., 2008, 2010; Ou et al., 2019) that the enriched source of alkaline melts, including high-K ones, in the metasomatized lithospheric mantle was a suite of amphibole- and phlogopite-bearing veins that were formed by metasomatic interaction between mantle peridotites and melting products of terrigenous sediments in a suprasubductional setting, with the involvement of fluids. A geochemical indication that such a source contributed to the generation of the melts is the higher concentrations of such elements that can be mobilized by fluid as K, Rb, Ba, Pb, and Sr than the concentrations of other incompatible elements, as well as elevated $^{87}Sr/^{86}Sr$ ratios, in rocks formed with the participation of such a source. The involvement of metasomatized lithospheric mantle most obviously follows from the isotope-geochemical features of the Potudan-type rocks.

CONCLUSIONS

Our data on the granitoids of three types of the Khokhol–Repyevka batholith show differences in their Sr and Nd isotope composition. The Potudan-type granites have low $\varepsilon_{Nd}(t)$ = −1.7 to −3.8 and initial $^{87}Sr/^{86}Sr(i)$ of 0.70381 to 0.70910; the Pavlovsk-type granitoids $\varepsilon_{Nd}(t)$ = +0.2to −3.7 and $^{87}Sr/^{86}Sr(i)$ = 0.70269–0.70309; and the hybrid rocks have $\varepsilon_{Nd}(t)$ = −8.8 and $^{87}Sr/^{86}Sr(i)$ = 0.70596.

The high Ba, Sr, and K concentrations, and the low $^{143}Nd/^{144}Nd$ and high $^{87}Sr/^{86}Sr$ ratios of the Potudan-type rocks indicate that their sources occurred in the metasomatized lithospheric mantle. The more radiogenic Nd isotope composition of the Potudan-type rocks in the northern massifs of the batholith was affected by mixing with Pavlovsk-type magmas.

The elemental and isotope geochemistry of the rocks of the Khokhol–Repyevka batholith indicate that it hosts two suites of leucogranite dikes: (1) those with εNd(t) = −3.8 and fractionated HREE patterns, (Gd_N/Yb_N=2.1–3.8), which might have been formed by the profound differentiation of Pavlovsk-type magma, and (2) leucogranites with εNd(t) = −7.8 and not so much fractionated HREE patterns REE (Gd_N/Yb_N=1.1–1.6), which were produced via the melting of the Archean crust of the Kursk block at relatively shallow depths.

The thermodynamic simulations of contamination of the Pavlovsk- and Potudan-type magmas with Archean gneisses confirm that the contamination model is able to explain the low εNd(t) of some of the dike leucogranites. The isotope composition of the rocks could be radically modified only by the mixing of compositionally contrasting compositions: the addition of much anatectic melt derived from the Archean crust of the Kursk block to the mafic melt.

The granitoids of the Khokhol–Repyevka batholith were formed with the involvement of melts generated by the partial melting of the following three sources: (1) lower crust (or buried oceanic crust) of dominantly mafic composition and/or enriched mantle that has been metasomatized in the Proterozoic, whose involvement is reflected in the composition of the Pavlovsk-type granitoids; (2) an enriched mantle source, which was likely subcontinental lithospheric mantle, that might have been metasomatized during the earlier geological evolution of the region, as is typical of the Potudan-type monzonitoids; and (3) Archean crust that was dominated by TTG gneisses and metasediments and underwent melting.

Supplementary 1. Representative chemical analyzes of rocks from the Khokhol-Repyevka batholith

Table 4

Hole/depth	Potudan type											
	7577/185	6418/66	7763/207.5	7586/280	7577/170	7769/201	7769/186	8003/365	7583/240	7578/150	7580/239.5	7577/145
SiO_2	46.95	50.82	53.62	53.86	53.98	54.31	56.05	58.47	61.51	61.23	62.91	64.07
TiO_2	1.87	2.30	1.04	1.39	0.93	0.91	0.84	1.27	0.79	0.80	0.94	0.80
Al_2O_3	15.69	13.86	14.91	15.96	13.90	18.60	18.11	14.45	14.04	15.96	14.57	14.46
FeO(tot)	13.34	13.65	12.08	10.93	12.35	8.64	7.20	8.78	7.75	6.17	5.78	6.06
MnO	0.14	0.13	0.16	0.14	0.16	0.12	0.10	0.08	0.09	0.09	0.09	0.07
MgO	5.14	3.53	4.92	3.62	3.32	3.07	3.11	2.91	3.28	2.67	2.87	2.30
CaO	7.77	7.44	6.45	8.17	8.13	6.05	6.16	6.40	5.59	5.49	5.01	4.88
Na_2O	3.58	3.07	3.65	3.76	3.08	4.55	4.72	3.72	3.64	4.50	4.09	3.45
K_2O	3.22	3.64	2.44	1.30	3.48	2.78	2.74	3.05	2.57	2.55	3.21	3.39
P_2O_5	1.84	1.44	0.57	0.61	0.49	0.64	0.60	0.70	0.27	0.42	0.45	0.43
Total	99.55	99.88	99.85	99.74	99.81	99.67	99.62	99.84	99.52	99.88	99.93	99.90
P	7869	6197	2485	2638	2114	2769	2616	3048	1162	1830	1961	1852
Ti	10952	13641	6192	8257	5491	5401	4988	7563	4665	4778	5599	4749
V	219	176	102	220	190	148	143	108	134	81	97	110
Cr	88.1	57	177	65.9	77.4	38.2	23.3	44.0	70.9	34.0	26.7	31.4
Co	11.0	2.84	14.0	26.7	13.0	20.6	8.00	6.00	10.00	6.00	4.00	4.00
Ni	31.2	22.9	34.0	21.9	18.9	10.8	9.54	27.0	24.8	18.0	12.0	6.89
Cu	48.7	21.4	12.0	44.4	35.6	22.8	41.4	20.0	51.4	4.00	9.22	6.39
Zn	157	81	69.0	103	119	104	95.9	76.0	78.1	47.0	79.1	64.6
Ga	28.4	24.0	16.0	26.4	24.9	31.5	24.9	17.0	21.0	18.0	22.3	22.3
Rb	80.3	82.6	123	34.5	35.9	95.3	66.2	53.0	83.9	69.0	84.6	63.1
Sr	1770	890	436	1030	1390	2020	1500	755	710	582	1120	1070
Y	21.3	33.2	14.0	21.9	22	11.2	11.7	16.0	18.3	11.0	13.6	11.7
Zr	66.0	530	133	76.0	136	212	201	93.0	89.0	100	107	109
Nb	20.7	27.3	18.0	10.9	14.6	10.7	8.42	14.0	13	9.00	9.72	9.02
Mo	1.21	2.29	–	1.06	–	0.85	3.52	–	0.61	–	–	0.75
Sn	3.00	–	5.00	1.3	–	1.34	1.00	3.00	–	3.00	2.00	–
Cs	9.00	14.172	5.00	1.49	6.00	1.01	6.00	11.0	6.00	5.00	6.00	5.00
Ba	2150	1510	1115	678	2040	3060	2190	1920	693	854	1390	1730
La	87.9	98.8	–	33.5	35.1	83.1	62.3	62.1	27.8	–	45.4	82.1
Ce	201	203	15.0	73.7	92.2	150	119	119	61.5	94.0	86.6	139
Pr	26.0	24.7	–	9.49	13.6	17.1	14	14.5	8.00	–	10.4	13.8

Table 4 (Contd.)

Nd	102	96.1	–	39.1	57.0	58.7	52.2	55.3	33.2	–	40.3	45.9
Sm	16.2	16.4	–	6.89	11.6	9.02	7.68	9.39	6.81	–	7.47	6.45
Eu	3.55	3.59	–	2.21	2.7	3.39	2.46	2.97	1.46	–	1.68	1.84
Gd	10.1	12.0	–	6.34	8.06	5.62	5.07	7.08	5.21	–	5.00	4.4
Tb	1.15	1.57	–	0.84	1.03	0.65	0.57	0.89	0.73	–	0.59	0.51
Dy	5.00	7.14	–	4.26	4.90	2.62	2.66	4.49	3.67	–	2.88	2.38
Ho	0.77	1.23	–	0.79	0.81	0.43	0.47	0.78	0.68	–	0.49	0.42
Er	1.98	3.35	–	2.41	2.04	1.24	1.2	1.98	1.87	–	1.34	1.16
Tm	0.23	0.4	–	0.31	0.27	0.13	0.15	0.26	0.26	–	0.18	0.17
Yb	1.35	2.57	–	1.57	1.47	0.86	1.00	1.56	1.64	–	1.08	1.06
Lu	0.16	0.37	–	0.23	0.22	0.11	0.14	0.21	0.24	–	0.16	0.16
Hf	3.32	10.4	–	3.5	6.38	7.4	7.94	3.51	4.14	–	4.89	11.2
Ta	1.16	1.51	–	0.62	0.95	0.39	0.64	1.09	0.85	–	0.35	0.74
Th	7.56	7.20	6.00	2.66	5.93	5.24	5.14	8.74	5.63	9.00	3.44	13.9
U	2.05	1.40	8.00	0.72	2.36	0.73	1.55	1.95	2.09	9.00	0.76	2.87
Th/Yb	5.6	2.80	–	–	–	–	–	5.60	–	–	–	–
Ta/Yb	0.9	0.59	–	–	–	–	–	0.70	–	–	–	–
Eu/Eu*	0.79	0.75	–	1.01	0.81	1.36	1.1	1.1	0.72	–	0.79	1.00
(La/Sm)N	3.41	3.79	–	3.06	1.90	5.80	5.1	4.2	2.57	–	3.82	8.01
(La/Yb)N	43.9	25.9	–	14.4	16.1	65.1	42.0	26.8	11.4	–	28.3	52.2
(GdYb)N	6.04	3.77	–	3.26	4.42	5.27	4.1	3.7	2.56	–	3.74	3.35
Hole/depth	Potudan type	Pavlov type					Hybrid type					
	8003/190	7763/200.5	7580/225	6432/86.7	7583/245	7770/210	7576/183	7576/190	6434/102	8003/295	6424/67	7576/200
SiO_2	64.34	60.14	65.55	68.24	72.04	73.09	52.51	53.94	56.80	61.41	66.39	69.03
TiO_2	0.46	0.70	0.54	0.34	0.28	0.20	1.82	1.58	0.74	0.93	0.71	0.07
Al_2O_3	15.86	16.17	14.94	13.63	13.70	13.68	14.79	14.27	15.68	14.80	14.88	13.80
FeO(tot)	6.28	6.75	4.26	5.74	2.26	1.81	10.70	10.46	9.05	7.16	4.86	3.97
MnO	0.09	0.09	0.05	0.07	0.00	0.02	0.14	0.12	0.13	0.10	0.04	0.10
MgO	1.46	2.94	1.63	0.81	0.63	0.52	3.42	3.72	3.75	2.78	0.73	1.31
CaO	4.00	5.88	3.25	3.72	2.44	2.19	7.02	6.49	6.62	5.49	1.60	1.10
Na_2O	4.73	4.28	3.66	3.86	3.36	3.39	3.37	3.44	3.59	3.55	2.67	2.55
K_2O	2.53	2.53	5.71	3.34	4.87	4.99	4.19	4.38	3.22	3.39	7.85	7.83
P_2O_5	0.26	0.36	0.32	0.22	0.09	0.06	1.41	1.20	0.29	0.33	0.25	0.07

Table 4 (Contd.)

Total	100.00	99.85	99.92	99.98	99.67	99.94	99.38	99.60	99.86	99.95	99.96	99.82
P	1114	974	891	1729	576	240	6061	5175	1249	1441	1057	301
Ti	2713	2006	2467	4114	2383	1174	10760	9323	4377	5527	4198	395
V	67	191	49.7	115	58.0	22.0	142	163	173	118	66.1	15.0
Cr	55.0	64.9	39.1	64.3	51.6	17.0	83.5	103	130	108	70.3	40.1
Co	0.00	–	1.00	11	–	–	8.00	27.9	25.4	11.0	6.62	2.00
Ni	15.8	8.00	11.0	31.0	10.0	11.0	34.5	32.3	21.7	34.0	7.68	20.1
Cu	4.17	1.00	1.00	14.0	3.00	2.00	63.9	43.3	27.5	10.0	12.6	36.1
Zn	85.0	59.0	26.0	68.0	44.0	12.0	124	136	78.5	73.0	45.2	45.2
Ga	22.0	23.2	18.1	18.1	14.7	12.0	29.9	29.3	24.8	18.5	22.7	17.0
Rb	66.2	87.0	82.8	102	80.5	70.0	71.5	77.6	135	118	177	127
Sr	380	912	650	780	658	501	883	1370	693	597	483	729
Y	21.8	32.8	16.1	33	2.95	1.00	26.1	42.5	19.9	10.6	22.6	2.44
Zr	208	151	74.0	99.0	60.0	55.0	249	307	162	186	296	–
Nb	10.2	30.2	18.0	23.6	4.33	4.00	30.7	62.1	13.5	9.15	27.9	6.05
Mo	1.71	2.50	1.56	–	–	–	1.03	1.76	2.41	2.02	3.85	1.51
Sn	–	4.00	–	5.00	–	–	3.00	3.46	1.44	–	1.34	–
Cs	3.159	3.00	3.00	6.00	2.00	1.00	12.0	0.40	4.72	7.00	1.15	–
Ba	505	1370	659	1010	572	406	2180	3100	1100	845	2270	3930
La	39.1	94.3	106	49.2	23.9	–	130	165	45.4	53.5	204	66.7
Ce	76.6	190	201	111	38.5	193	258	377	85.6	93.5	370	110
Pr	9.18	24.1	21.0	14.8	3.85	–	30.3	47.9	9.93	9.38	38.3	10.9
Nd	33.8	91.9	68.6	58.3	13.0	–	109	172	35.5	31.3	112	33.8
Sm	6.53	15.9	9.23	11.2	1.87	–	17.7	23.1	5.81	4.68	12.3	4.29
Eu	1.28	3.22	1.80	2.05	1.15	–	4.30	5.98	1.61	1.34	2.66	1.79
Gd	5.44	11.5	5.64	9.13	1.11	–	10.9	17.3	4.96	3.87	9.29	2.09
Tb	0.79	1.51	0.66	1.16	0.14	–	1.29	2.07	0.77	0.50	1.12	0.19
Dy	4.36	6.97	3.43	5.90	0.57	–	5.68	9.34	3.76	2.36	4.82	0.63
Ho	0.73	1.13	0.58	1.14	0.10	–	0.97	1.61	0.76	0.43	0.78	0.098
Er	2.09	3.23	1.56	3.12	0.25	–	2.40	4.41	2.18	0.96	2.54	0.25
Tm	0.27	0.43	0.22	0.43	0.04	–	0.30	0.52	0.24	0.14	0.25	0.026
Yb	1.38	2.50	1.32	2.76	0.22	–	1.79	3.36	1.88	0.80	1.55	0.15
Lu	0.22	0.34	0.2	0.4	0.03	–	0.25	0.42	0.28	0.15	0.22	0.023
Hf	5.57	7.97	4.17	3.71	2.47	–	9.19	13.5	4.98	5.35	11.6	0.28
Ta	0.37	1.51	1.54	2.11	0.20	–	1.02	3.51	0.68	0.33	1.36	0.20

Table 4 (Contd.)

Th	3.53	7.08	30.9	20.8	3.52	6.00	6.28	8.95	13.1	12.4	31.1	33.1
U	0.92	1.46	2.10	4.89	0.53	9.00	0.96	1.40	2.21	2.01	1.89	0.71
Th/Yb	2.56	2.83	–	–	–	–	3.51	2.66	–	15.5	20.1	221
Ta/Yb	0.27	0.60	–	–	–	–	0.57	1.04	–	0.41	0.88	1.33
Eu/Eu*	0.64	0.70	0.71	0.60	2.26	–	0.88	0.88	–	0.94	0.73	1.62
(La/Sm)N	3.77	3.73	7.22	2.76	8.04	–	4.62	4.49	4.92	7.19	10.43	9.78
(La/Yb)N	19.1	25.4	54.1	12.0	73.2	–	49.0	33.1	–	45.1	88.7	300
(GdYb)N	3.18	3.71	3.45	2.67	4.07	–	4.91	4.15	–	3.90	4.84	11.24
	Hybrid type	Dike type				Liskinsky leucogranite type						
Hole/depth	7576/186	8003/160	6416/60.8	7769/209.3	6435/77	K-22/97.7	K-925-1/94.4	K-35/7.1	K-911-1/215	K-915-2/380.5	K-908/85.2	K-12/93.7
SiO_2	72.30	73.29	74.51	75.44	75.75	74.79	75.73	75.56	74.64	78.28	77.47	76.55
TiO_2	0.24	0.30	0.06	0.14	0.08	0.32	0.18	0.18	0.20	0.11	0.12	0.23
Al_2O_3	14.09	12.90	12.14	12.86	11.79	11.85	12.69	13.06	13.19	12.48	11.92	12.26
FeO(tot)	2.30	2.40	1.43	1.46	1.47	2.84	2.53	1.70	2.24	1.47	1.33	1.84
MnO	0.02	0.02	0.01	0.02	0.01	0.041	0.03	0.02	0.02	0.02	0.02	0.03
MgO	0.88	0.51	0.06	0.27	0.15	0.39	0.17	0.19	0.23	0.07	0.09	0.20
CaO	2.84	0.41	1.52	1.26	1.18	1.14	1.72	1.34	1.21	1.95	1.00	1.37
Na_2O	4.82	3.35	3.59	3.76	2.77	4.27	2.28	2.54	2.71	2.88	3.79	2.92
K_2O	2.23	6.72	6.59	4.70	6.77	4.31	4.63	5.37	5.52	2.71	4.24	4.57
P_2O_5	0.14	0.08	0.00	0.03	0.03	0.041	0.03	0.03	0.03	0.02	0.02	0.03
Total	99.87	99.98	99.91	99.95	99.98	100	100	100	100	100	100	100
P	616	–	131	349	109	–	–	–	–	–	–	–
Ti	1413	353	850	1790	503	–	–	–	–	–	–	–
V	25.0	14.0	17.0	21.0	29.6	–	–	–	–	–	–	–
Cr	34.0	44.0	21.0	23.0	57.1	–	–	–	–	–	–	–
Co	1.00	–	–	–	–	–	–	–	–	–	–	–
Ni	15	4.00	3.00	8.00	8.068	–	–	–	–	–	–	–
Cu	7.00	5.00	–	–	4.154	–	–	–	–	–	–	–
Zn	19.0	7.00	15.0	16.0	17.186	–	–	–	–	–	–	–
Ga	13.0	12.0	13.0	10.0	18.6	–	–	–	–	–	–	–
Rb	37.0	190	210	180	140	–	–	–	–	–	–	–
Sr	465	33	121	73	132	–	–	–	–	–	–	–
Y	1.00	7.00	3.00	9.00	0.59	–	–	–	–	–	–	–

Table 4 (Contd.)

Zr	88	39	76	157	48.068	–	–	–	–	–	–	–
Nb	4.00	22.0	11.0	12.0	1.58	–	–	–	–	–	–	–
Mo	–	–	–	–	1.51	–	–	–	–	–	–	–
Sn	3.00	2.00	1.00	2.00	4.00	–	–	–	–	–	–	–
Cs	2.00	–	49	29	0.36	–	–	–	–	–	–	–
Ba	339	86	230	387	406	–	–	–	–	–	–	–
La	–	–	–	–	14.1	–	–	–	–	–	–	–
Ce	81	54	71	280	20.00	–	–	–	–	–	–	–
Pr	–	–	–	–	1.81	–	–	–	–	–	–	–
Nd	–	–	–	–	4.31	–	–	–	–	–	–	–
Sm	–	–	–	–	0.28	–	–	–	–	–	–	–
Eu	–	–	–	–	0.29	–	–	–	–	–	–	–
Gd	–	–	–	–	0.27	–	–	–	–	–	–	–
Tb	–	–	–	–	0.05	–	–	–	–	–	–	–
Dy	–	–	–	–	0.09	–	–	–	–	–	–	–
Ho	–	–	–	–	0.01	–	–	–	–	–	–	–
Er	–	–	–	–	0.05	–	–	–	–	–	–	–
Tm	–	–	–	–	0.01	–	–	–	–	–	–	–
Yb	–	–	–	–	0.06	–	–	–	–	–	–	–
Lu	–	–	–	–	0.01	–	–	–	–	–	–	–
Hf	–	–	–	–	1.71	–	–	–	–	–	–	–
Ta	–	–	–	–	–	–	–	–	–	–	–	–
Th	6.00	15.0	–	–	18.8	–	–	–	–	–	–	–
U	8.00	5.00	–	–	2.91	–	–	–	–	–	–	–
Th/Yb	–	–	–	–	330	–	–	–	–	–	–	–
Ta/Yb	–	–	–	–	–	–	–	–	–	–	–	–
Eu/Eu*	–	–	–	–	3.18	–	–	–	–	–	–	–
(La/Sm)N	–	–	–	–	31.68	–	–	–	–	–	–	–
(La/Yb)N	–	–	–	–	166.77	–	–	–	–	–	–	–
(GdYb)N	–	–	–	–	3.82	–	–	–	–	–	–	–

Supplementary 2. Distribution coefficients of chemical elements in "mineral-melt systems" used in the work

Table 5

	Partition coefficients for minerals					
rock	andesite*					basalt**
element/mineral	Cpx	Ol	Pl	Ilm	Mag	Opx
Ba	0.07	0.02			0.26	
Dy	1.16	0.06	0.11		0.51	
Eu	0.82	0.03	0.57		0.32	
Gd	0.72		0.04			
Hf	0.37	0.02	0.02	0.38	0.46	0.05
La	0.25	0.01	0.18		0.34	
Nd	0.97	0.02	0.11		0.40	0.02
Sm	0.92	0.01	0.09		0.42	
Ni	6.80	26.33	0.30		14.30	
Rb	0.04	0.04	0.17		0.15	
Sr	0.45	0.03	3.42		0.11	
Ta	0.43		0.03	6.60		
Y	2.40				0.64	0.38
Th	0.10	0.02	0.03		0.24	0.00
Nb	2.10			4.60		0.00
Yb	1.18	0.03	0.05		0.36	0.16
Zr	0.30		0.18	0.2	0.38	0.01

(Cpx) clinopyroxene, (Ol) olivine, (Pl) plagioclase, (Ilm) ilmenite, (Mg) magnetite, (Opx) orthopyroxene.

*Average Kd values for minerals in andesites from works:

1) Green T.H., Pearson, N.J. (1985). Rare Earth element partitioning between clinopyroxene and silicate liquid at moderate to high pressure. *Contributions to Mineralogy and Petrology.* (91), 24–36.

2) Anderson, A.T., Greenland, L.P. **(1969).** Phosphorous fractionation diagrams as a quantitative indicator of crystallization differentiation of basaltic liquids. *Geochimica et Cosmochimica Acta*. (**33**), 493–505. doi: 10.1016/0016- 7037(69)90129-X.

3) Luhr J.F., Carmichael I.S.E. (1980). The Colima volcanic complex, Mexico. I: postcaldera andesites from Volcan Colima. *Contributions to Mineralogy and Petrology.* **(71),** 343–372.

4) Ewart A., Griffin W.L. (1994). Application of Proton-Microprobe Data to Trace- Element Partitioning in Volcanic-Rocks. *Chemical Geology.* **117** (1–4), 251–284. doi: 10.1016/0009-2541(94)90131-7.

5) Bacon C.R., Druitt T.H. (1988). Compositional Evolution of the Zoned Calcalkaline Magma Chamber of Mount-Mazama, Crater Lake, Oregon. *Contributions to Mineralogy and Petrology.* **98** (2), 224–256.

**Average Kd values for orthopyroxene in basalts from works:

1) Bindeman I., Davis A. (2000). Trace element partitioning between plagioclase and melt: Investigation of dopant influence on partition behavior. *Geochimica et Cosmochimica Acta.* (**64**), 2863-2878. doi: 10.1016/S0016-7037(00)00389-6.

2) Schwandt C.S., McKay G.A. (1998) Rare earth element partition coefficients from enstatite/melt synthesis experiments. Geochimica et Cosmochimica Acta **62**(16). 2845–2848. doi: 10.1016/S0016-7037(98)00233-6.

ACKNOWLEDGMENTS

The authors thank M.V. Luchitskaya and the anonymous reviewer for attention to the manuscript and valuable criticism, which led us to improve this publication.

FUNDING

This work was supported by ongoing institutional funding, project FMUW-2022-0002 for the Institute of Precambrian Geology and Geochronology, Russian Academy of Sciences. No additional grants to carry out or direct this particular research were obtained.

CONFLICT OF INTEREST

The authors declare that they have no conflicts of interest.

REFERENCES

C. Annen, J. D. Blundy, and R. S. J. Sparks, "The sources of granitic melt in deep hot zones," Trans. R. Soc. Edinburgh: Earth Sci. **97**, 297–309 (2008).

A. A. Ariskin, L. V. Danyushevskii, E. G. Konnikov, R. Maas, Yu. A. Kostitsyn, E. Mak-Nil, S. Meffre, G. S. Nikolaev, and E. V. Kislov, "The Dovyren intrusive complex (northern Baikal region, Russia): isotope-geochemical

markers of contamination of parental magmas and extreme enrichment of the source," Russ. Geol. Geophys. **56** (3), 528–556 (2015).

P. D. Asimow and M. S. Ghiorso, "Algorithmic modifications extending MELTS to calculate subsolidus phase relations," Am. Mineral. **83**, 1127–1131 (1998).

E. V. Bibikova, S. V. Bogdanova, A. V. Postnikov, A. A. Fedotova, S. Klaesson, T. I. Kirnozova, M. M. Fugzan, and L. P. Popova, "The early crust of the Volgo-Uralian segment of the East European Craton: isotope-geochronological zirconology of metasedimentary rocks of the Bolshecheremshanskaya Formation and their Sm-Nd model ages," Stratigraphy. Geol. Correlation **23** (1), 1–23 (2015).

E. V. Bibikova, S. V. Bogdanova, A. V. Postnikov, L. P. Popova, T. I. Kirnozova, M. M. Fugzan, and V. V. Glushchenko, "Sarmatia–Volgo-Uralia junction zone: isotopic–geochronologic characteristic of supracrustal rocks and granitoids," Stratigraphy. Geol. Correlation **17** (6), 561–573 (2009).

R. Black and J. P. Liegéois, "Cratons, mobile belts, alkaline rocks and continental lithospheric mantle; the Pan-African testimony," J. Geol. Soc. London **150**, 89–98 (1993).

S. V. Bogdanova, R. Gorbatschev, and R. G. Garetsky, *East European Craton*. *Encyclopedia of Geology*, Ed. by R. Selley, R. Cocks, I. Plimer (Elsevier, Amsterdam, 2005), Vol. 2, pp. 34–49.

W. A. Bohrson, F. J. Spera, M. S. Ghiorso, G. A. Brown, J. B. Creamer, and A. Mayfield, "Thermodynamic model for energy-constrained open-system evolution of crustal magma bodies undergoing simultaneous recharge, assimilation and crystallization: the magma chamber simulator," J. Petrol. **55**, 1685–1717 (2014). https://doi.org/10.1093/petrology/egu036

B. Bonin, A. Azzouni-Sekkal, F. Bussy, and S. Ferrag, "Alkali-calcic and alkaline postorogenic (PO) granite magmatism: petrologic constraints and geodynamic settings," Lithos **45**, 45–70 (1998).

A. O. Chaves, "Columbia (Nuna) supercontinent with external subduction girdle and concentric accretionary, collisional and intracontinental orogens permeated by large igneous provinces and rifts," Precambrian Res. **352**, (2021). https://doi.org/10.1016/j.precamres.2020.106017

K. C. Condie, "Preservation and recycling of crust during accretionary and collisional phases of proterozoic orogens: a bumpy road from Nuna to Rodinia," Geosciences **3**, 240–261 (2013).

J. A. Connolly, "Multivariable phase–diagrams – an algorithm based on generalized thermodynamics," Amer. J. Sci. **290**, 666–718 (1990).

F. Corfu, J. Hanchar, P. W.O. Hoskin, and P. Kinny, "Atlas of zircon textures," Rev. Mineral. Geochem. **53**, 59 (2003).

O. I. Egipko, Candidate's Dissertation in Geology and Mineralogy (Voronezh, 1971) [in Russian].

A. A. Fedotova, S. V. Bogdanova, S. Klaesson, M. O. Anosova, A. V. Postnikov, M. M. Fugzan, and T. I. Kirnozova, "New data on the Paleoproterozoic age of metamorphism in the Yelabuga deformation zone of Volgo-Uralia, East European Craton," Dokl. Earth Sci. **488** (3), 1123–1127 (2019).

B. R. Frost, C. G. Barnes, W. J. Collins, R. J. Arculus, D. J. Ellis, and C. D. Frost, "A geochemical classification for granitic rocks," J. Petrol. **42** (11), 2033–2048 (2001).

M. S. Ghiorso and R. O. Sack, "Chemical mass transfer in magmatic processes IV. A revised and internally consistent thermodynamic model for the interpolation and extrapolation of liquid-solid equilibria in magmatic systems at elevated temperatures and pressures," Contrib. Mineral. Petrol. **119**, 197–212 (1995). https://doi.org/10.1007/bf00307281

S. J. Goldstein and S. B. Jacobsen, "Nd and Sr isotopic systematics of river water suspended material: implications for crustal evolution," Earth Planet. Sci. Lett. **87**, 249–265 (1988).

I. M. Gorokhov, N. N. Melnikov, A. B. Kuznetsov, G. V. Konstantinova, and T. L. Turchenko "Sm–Nd systematics of fine-grained fractions of the Lower Cambrian blue clay in northern Estonia," Lithol. Miner. Resour. **42** (5), 482–495 (2007).

I. M. Gorokhov, T. S. Zaitseva, A. B. Kuznetsov, G. V. Ovchinnikova, M. M. Arakelyants, V. P. Kovach, G. V. Konstantinova, T. L. Turchenko, and I. M. Vasileva, "Isotope systematics and age of authigenic minerals in shales of the Upper Riphean Inzer Formation, South Urals," Stratigraphy. Geol. Correlation **27** (2), 133–158 (2019).

Z. Guo, M. Wilson, J. Liu, and Q. Mao, "Post-collisional, potassic and ultrapotassic Magmatism of the Northern Tibetan Plateau: constraints on characteristics of the mantle source, geodynamic setting and uplift mechanisms," J. Petrol. **47** (6), 1177–1220. doi:10 (2006).1093/petrology/egl007

H. E. Huppert and R. S.J. Sparks, "The generation of granitic magmas by intrusion of basalt into continental crust," J. Petrol. **29**, 599–624 (1988).

S. B. Jacobsen and Wasserburg. G.J., "Sm-Nd evolution of chondrites and achondrites," Earth Planet. Sci. Lett. **67**, 137–150 (1984).

N. V. Koronovsky and N. A. Yasamanov, Earth Planet. Physicochemical Composition and Aggregate State of the Earth's Substance. Geology: A Textbook for Students, 8th Ed., (Akademiya, Moscow, 2012) [in Russian].

A. B. Kuznetsov, S. B. Lobach-Zhuchenko, T. V. Kaulina, and G. V. Konstantinova, "Paleoproterozoic age of carbonates and trondhjemites of the Central Azov Group: Sr isotope chemostratigraphy and U–Pb geochronology" Dokl. Earth Sci. **484** (2), 142–145 (2019).

O. Laurent, H. Martin, J. F. Moyen, and R. Doucelance, "The diversity and evolution of late-Archean granitoids: evidence for the onset of 'modern-style' plate tectonics between 3.0 and 2.5 Ga," Lithos **205**, 208–235 (2014). https://doi.org/10.1016/j.lithos.2014.06.012

J. G. Meert, "What's in a name? The Columbia (Paleopangaea/Nuna) supercontinent," Gondwana Res. **21** (4), 987–993 (2012).

E. A.K. Middlemost, "Naming materials in the magma/igneous rock system," Earth Sci. Rev. **37**, 215–224 (1994).

M. V. Mints, V. N. Glaznev, and O. M. Muravina, "Deep structure of the crust of the southeastern Voronezh-crystalline massif based on geophysical data: geodynamic evolution in the Paleoproterozoic and the modern state of the crust," Vestn. Voronezhsk. Gos. Univ. Ser. Geol., No. 4, 5–23 (2017).

J. T. O'Connor, "A classification of quartz-rich igneous rocks based on feldspar ratios," U.S. Geol. Surv. Prof. Pap. **525-B**, 79–84 (1965).

Q. Ou, Q. Wang, D. A. Wyman, C. Zhang, L-L. Hao, W. Dan, Z-Q. Jiang, F-Y. Wu, J-H. Yang, H-X. Zhang, X-P. Xia, L. Ma, X-P. Long, and J. Li, "Postcollisional delamination and partial melting of enriched lithospheric mantle: Evidence from Oligocene (ca. 30 Ma) potassium-rich lavas in the Gemuchaka area of the central Qiangtang Block, Tibet," Geol. Soc. Am. Bull. **131** (7/8). 1385–1408 (2019). https://doi.org/10.1130/B31911.1

A. E. Patino-Douce and J. S. Beard, "Dehydration melting of biotite gneiss and quartz amphibolite from 3 to 15 kbars," J. Petrol. **36**, 707–738 (1995).

M. E. Petrakova and R. A. Terentev, "Petrographic and mineralogical features of interaction of the granitoid and gabbroid magmas of the Potudan Pluton, Voronezh crystalline massif," Vestn. Voronezhsk. Gos. Univ. Ser. Geol., No. 1, 32–45. https://doi.org/ (2018). https://doi.org/10.17308/geology.2018.1/1422

M. E. Petrakova, R. A. Terentev, A. V. Yurchenko, and K. A. Savko, "Geochemistry and geochronology of the Paleoproterozoic quartz monzogabbro–monzodiorite–granodiorite pluton, Volga–Don orogen," Vestn, SPbGU: Nauki o Zemle. 67 (1), 74–96 (2022a). https://doi.org/10.21638/spbu07.2022.105

M. E. Petrakova, R. L. Anisimov, and Sh. K. Baltybaev, "Conditions of formation of magmatic rocks of the Khokholsk-Repevsk batholith of the Volga–Don orogen: verification of models of fractional crystallization and assimilation," Tr. Fersman. Nauchn. Sessii GI KNTs RAN **19**, 284–289 (2022b). doi.org/ https://doi.org/10.31241/FNS.2022.19.052

S. Pilet, P. Ulmer, and S. Villiger, "Liquid line of descent of a basanitic liquid at 1.5 GPa: Constraints on the formation of metasomatic veins," Contrib. Mineral. Petrol. **159** (5), 621–643 (2010) https://doi.org/10.1007/s00410-009-0445–y

S. Pillet, M. B. Baker, and E. M. Stolper, "Metasomatized lithosphere and the origin of alkaline lavas," Science **320**, 1–10 (2008). https://doi.org/10.1126/science.1156563

Q. Qian and J. Hermann, "Partial melting of lower crust at 10–15 kbar: constraints on adakite and TTG formation," Contrib. Mineral. Petrol. **165**, 1195–1224 (2013).

F. Ridolfi, A. Renzulli, and M. Puerini, "Stability and chemical equilibrium of amphibole in calc-alkaline magmas: an overview, new thermobarometric formulations and application to subduction-related volcanoes," Contrib. Mineral. Petrol. **160**. 45–66 (2010).

K. A. Samsonov A.V. Savko, E. B. Salnikova, A. B. Kotov, and N. S. Bazikov, "HT/LP metamorphic zoning in the eastern Voronezh Crystalline Massif: Age and parameters of metamorphism and its geodynamic environment," Petrology **23** (6), 559–575 (2015).

K. A. Savko, A. V. Samsonov, and N. S. Bazikov, "Metaterrigenous rocks of the Vorontsovka Group of the Voronezh crystalline massif: geochemistry, formation, and source areas," Vestn. Voronezhsk. Gos. Univ., Ser. Geol., No. 1, 70–94 (2011).

K. A. Savko, A. V. Samsonov, A. N. Larionov, Yu. O. Larionova, and N. S. Bazikov, "Paleoproterozoic A- and S-granites in the Eastern Voronezh Crystalline Massif: geochronology, petrogenesis, and tectonic setting of origin," Petrology **22** (3), 205–233 (2014).

K. A. Savko, A. V. Samsonov, E. B. Salnikova, A. V. Kotov, and N. S. Bazikov, "HT/LP metamorphic zoning in the Eastern Voronezh Crystalline Massif: age and parameters of metamorphism and its geodynamic environment," Petrology **23** (6), 559–575 (2015).

A. V. Samsonov, V. A. Spiridonov, Yo. O. Larionova, A. N. Larionov, E. V. Bibikova, and V. Y. Gerasimov, "Pleoproterozoic history of assemblage of the East European Craton: Evidence from basement of the Russian platform," In *Moscow International School of Earth Sciences. Abstracts of International Conference* (Eds. L.N. Kogarko). (Vernadsky Institute of Geochemistry and Analytical Chemistry RAS Vernadsky State Geological Museum RAS Lomonosov Moscow State University, Moscow, 2016), pp. 21–22 [in Russian].

K. A. Samsonov A.V. Savko, A. N. Larionov, E. Kh. Korish, and N. S. Bazikov, "An Archaean tonalite–trondhjemite–granodiorite association of the Kursk Block (Voronezh Massif): composition, age, and correlation with the Ukrainian Shield," Dokl. Earth Sci. **478** (1), 115–119 (2018).

K. A. Savko, A. V. Samsonov, A. B. Kotov, E. B. Sal'nikova, E. H. Korish, A. N. Larionov, I. V. Anisimova, and N. S. Bazikov, "The Early Precambrian metamorphic events in eastern Sarmatia," Precambrian Res **311**, 1–23 (2018).

K. A. Savko, A. V. Samsonov, M. A. Golunova, K.-L. Vong, N. S. Bazikov, N. V. Kholina, and T. N. Polyakova, "Paleoarchean TTG and metapelites – protoliths of the Neoarchean A-type rhyolites of the Kursk block of Sarmatia: results of experiments on the dehydratational melting," Vestn. Voronezhsk. Gos. Univ., Ser. Geol., No. 2, 29–40 (2021). https://doi.org/10.17308/geology.2021.2/3486

A. A. Shchipansky, A. V. Samsonov, A. Yu. Petrova, and Yu. O. Larionova, "Geodynamics of the eastern margin of Sarmatia in the Paleoproterozoic," Geotectonics **41** (1), 38–62 (2007).

A. A. Shchipansky and T. N. Kheraskova, "The Volga–Don collisional orogen in the East European Craton as a Paleoproterozoic analog of the Himalayan–Tibetan Orogen," Geodynamics & Tectonophysics **14** (2), 1–21 (2023). https://doi.org/10.5800/GT-2023-14-2–0692

S. S. Sun and W. F. McDonough, "Chemical and isotopic systematic of oceanic basalts: implications for mantle composition and processes," Geol. Soc. Lon. Spec. Publ. **42**, 313–345 (1989).

P. J. Sylvester, "Post-collisional alkaline granites," J. Geol. **97**, 261–280 (1989).

R. A. Terentiev, "Paleoproterozoic sequences and magmatic complexes of the Losevo suture zone of the Voronezh

Crystalline Massif: geological position, material composition, geochemistry, and paleogeodynamics,"Stratigraphy Geol. Correlation **22** (2), 123–146 (2014).

R. A Terentiev, "Petrography and geochronology of granites of the Liskin plutona of the Voronezh crystalline massif," Vestn. Voronezhsk. Gos. Univ., Ser. Geol., No. 3, 43–52 (2016).

R. A. Terentiev, "Geology of the Precambrian Don Group of the Voronezh Crystalline Massif," Vestn. Voronezhsk. Gos. Univ., Ser. Geol., No. 2, 5–19 (2018).

R. A. Terentiev and M. Santosh, "Detrital zircon geochronology and geochemistry of metasediments from the Vorontsovka terrane: implications for microcontinent tectonics, Int. Geol. Rev. **58**, 1108–1126 (2016).

R. A. Terentev and K. A. Savko, "Mineral thermobarometry and geochemistry of Paleoproterozoic magnesian–potassic granitoids of the Pavlovsk pluton, East European Craton," Vestn. Voronezhsk. Gos. Univ., Ser. Geol., No. 3, 34–45 (2017).

R. A. Terentiev, K. A. Savko, and M. Santosh, "Paleoproterozoic evolution of the arc-back-arc system in the East Sarmatian Orogen (East European Craton): Zircon SHRIMP geochronology and geochemistry of the Losevo Volcanic Suite," Am. J. Sci. **317**, 707–753 (2017).

R. A. Terentiev, K. A. Savko, M. E. Petrakova, M. Santosh, and E. H. Korish, "Paleoproterozoic granitoids of the Don terrane, East-Sarmatian Orogen: age, magma source and tectonic implications," Precambrian Res. **346**, 1–24 (2020). https://doi.org/10.1016/j.precamres.2020.105790

G. Topuz, R. Altherr, W. H. Schwarz, W. Siebel, M. Satir, and A. Dokuz, "Postcollisional plutonism with adakite-like signatures: the Eocene Saraycik granodiorite (Eastern Pontides, Turkey)," Contrib. Mineral. Petrol. **150**, 441–455 (2005).

O. M. Turkina and I. N. Kapitonov, "The source of Paleoproterozoic collision granitoids (Sharyzhalgai Uplift, Southwestern Siberian Craton): from lithospheric mantle to upper crust," Russ. Geol. Geophys. **60**, 414–434 (2019).

G. Vrown, R. S. Thorpe, and P. C. Webb, "The geochemical characteristics of granitoids in contrasting arcs and comments on magma sources," J. Geol. Soc. **141** (3), 413–426 (1984).

J. M. Watkins, J. D. Clemens, and P. J. Treloar, "Archaean TTGs as sources of younger granitic magmas: melting of sodic metatonalites at 0.6±1.2 GPa," Contrib. Mineral. Petrol. **154**, 91–110.
DOI: 10 (2007).1007/s00410-007-0181–0

J. C. White, D. F. Parker, and M. Ren, "The origin of trachyte and pantellerite from Pantelleria, Italy: insights from major element, trace element and thermodynamic modelling," J. Volcanol. Geotherm. Res. **179**, 33–55 (2009).

D. L. Whitney and B. W. Evans, "Abbreviations for names of rock-forming minerals," Am. Mineral. **95**, 185–187 (2010).

G. Zhao, P. A. Cawood, S. A. Wilde, and M. Sun, "Review of global 2.1–1.8 Ga orogens: implications for a pre-Rodinia supercontinent," Earth Sci. Rev. **59**, 125–162 (2002).

Translated by E. Kurdyukov

SPELL: OK